Review

Received: 22 May 2015 Revised: 4 August 2015 Accepted article published: 12 August 2015 Published online in Wiley Online Library: 4 September 2015

(wileyonlinelibrary.com) DOI 10.1002/jctb.4797

Multifunctional graphene-based nanostructures for efficient electrocatalytic reduction of oxygen

Peiguang Hu, Ke Liu, Christopher P Deming and Shaowei Chen*

Abstract

Graphene derivatives have been used extensively as a functional support for nanoparticle catalysts in diverse applications, in particular, oxygen reduction reactions (ORR) at fuel cell cathodes. This review summarizes recent progress in this area of research, where the catalytic performance is evaluated within the context of stabilization of metal nanoparticles against sintering/aggregation and metal–substrate interactions that manipulate the electronic properties of metal nanoparticles and hence the bonding interactions with reaction intermediates. Also discussed are the latest breakthroughs of heteroatom-doped graphene derivatives as effective metal-free catalysts for oxygen reduction. In addition, the review includes a perspective on the development of effective ORR catalysts with a focus on a further understanding of the ORR mechanism as well as on other two-dimensional layered nanostructures such as MoS_2 that have been observed to exhibit electrocatalytic activity for oxygen reduction. Leading mechanistic models are discussed to account for the electrocatalytic activity.

Keywords: oxygen reduction reaction; electrocatalysis; graphene; nanoparticle; heteroatom-doped; MoS_2

INTRODUCTION

Fuel cell technologies have long been attracting extensive interest as a portable and renewable energy source.[1–4] However, this technology is currently limited in the commercial setting due to the high costs and relatively low efficiency of fuel cell catalysts, largely as a result of the sluggish kinetics of oxygen reduction at the fuel cell cathode,[5–7] $O_2 + 4H^+ + 4e \rightarrow 2H_2O$. Currently there are two leading models of oxygen reduction reaction (ORR), the direct and series pathways (Fig. 1).[8] The former entails the breaking of the oxygen–oxygen bond before protonation while the latter involves protonation of the adsorbed O_2 before bond breaking and further reduction.

Although the differences have significant impacts on the investigation of electrocatalysis, there are two important similarities worth examining further. First, each intermediate, regardless of the pathway, is bound to the catalyst surface through the oxygen atom. Second, the initial step involves adsorption of O_2 followed by an electron transfer, while the final step involves transfer of the last electron and removal of water. The first fact results in a linear correlation of the bonding interaction between a catalyst surface and an individual oxygen intermediate (OI). That is, any surface that will bind strongly to an OI will also interact strongly with the others. The consequence of the second fact is that facile adsorption *and* desorption are necessary for complete and efficient reduction. The overall significance of these two facts is that the best catalysis for ORR must exhibit *moderate* binding to oxygen and OIs.[9,10] In fact, theoretical studies, in conjunction with experimental work, have shown that Pt binds to OIs about 0.1 to 0.2 eV too strongly, whereas metals such as silver and gold do not interact appreciably with OIs and therefore are limited by the initial adsorption of water in oxygen reduction activity.[11–13]

This varying affinity to oxygen can be further related to the d band center relative to the Fermi level, and when plotted vs activity, shows a volcano shaped trend that was predicted by Sabatier years ago.[5,9,10,14–18] Figure 2 shows the activity of pure metals plotted against the difference between the d band center and the Fermi level ($\varepsilon_d - \varepsilon_f$). The metals showing strong interactions with OIs tend to have a high d band center relative to the Fermi level, while those with weaker interactions with OIs have a lower d band center. It is also clear that Pt is the most active metal but there is still room for improvement.

To reach the peak of this theoretical volcano, a number of strategies have been adopted. These include the formation of core/shell and homogeneous alloy nanoparticles,[5,10,11,19–22] size manipulation,[23–27] controlled growth of particle shape or facet orientation,[28–31] and organic functionalization.[32–36] In addition, techniques to improve and manipulate the role of the supporting substrate are also being developed and have shown promising results.[37–47]

Metal nanoparticle catalysts are generally deposited on a robust, high surface area, highly conducting substrate to provide maximum exposure of the metal surface and minimum charge transfer resistance to the electrode.[48,49] Carbon black (CB) is typically utilized; yet there are issues in terms of purity, stability, and sustained particle deposition. Such a carbon support is generally

* *Correspondence to: Shaowei Chen, Department of Chemistry and Biochemistry, University of California, 1156 High Street, Santa Cruz, California 95064, USA. E-mail: shaowei@ucsc.edu*

Department of Chemistry and Biochemistry, University of California, 1156 High Street, Santa Cruz, California 95064, USA

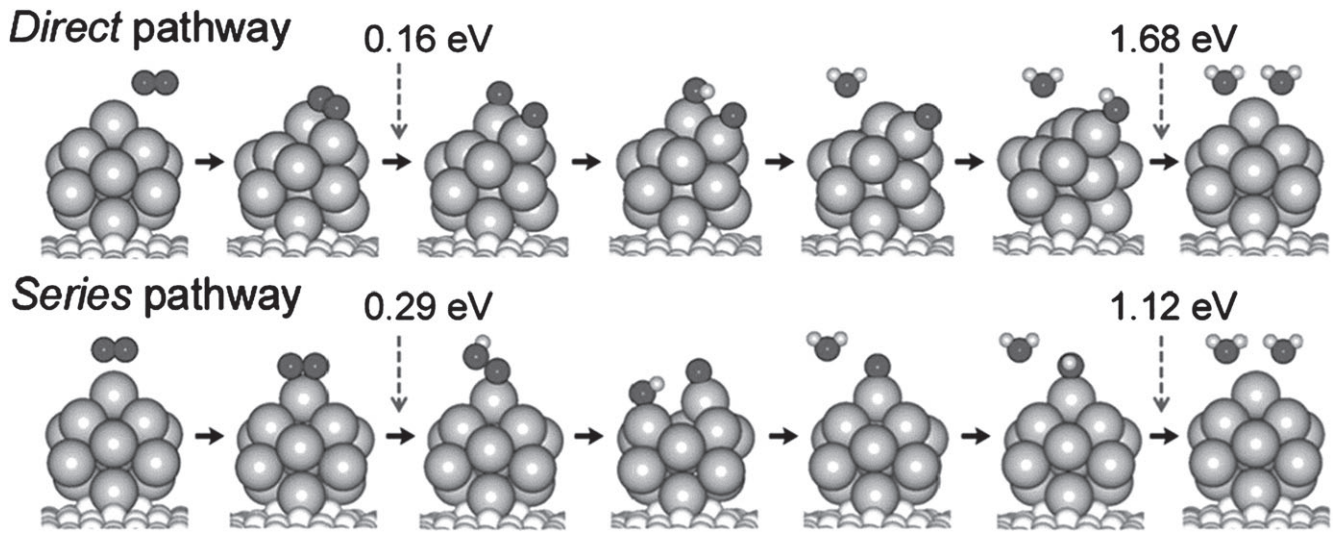

Figure 1. Direct and series pathways for oxygen reduction. Reproduced with permission from ref. 8.

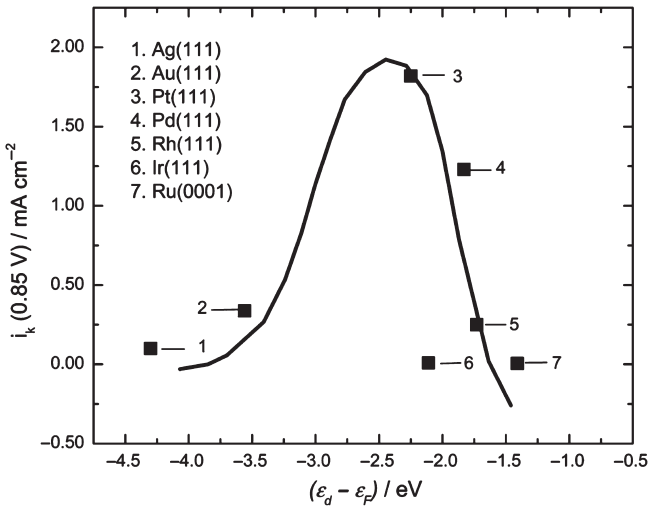

Figure 2. ORR specific activity of different metal (111) facets as a function of difference between d band center and Fermi level. Reproduced with permission from ref. 9.

used in acidic media because it has been found that continuous use in alkaline media will lead to corrosion and inactivity.[50] Thus, other carbon-based substrates are emerging, such as graphene, graphene oxide (GO), graphene quantum dots (GQDs),[44–47,51] mesoporous carbon,[39–41] and 1D materials such as carbon nanotubes and fibers.[37,38,42,43] Thus far, graphene-based supports have shown much improvement over the traditional carbon black displaying remarkable charge-transfer properties, high surface area, chemical inertness, and mechanical flexibility, and are therefore the focus of much research.[52]

Furthermore, the incorporation of heteroatoms into the graphitic structure has enabled efficient oxygen reduction without metal nanoparticle catalysts.[53–55] The doping of heteroatoms is thought to activate neighboring carbon atoms for oxygen adsorption and subsequent reduction.[56,57] Diverse methods have been reported for the synthesis of doped carbons with precise control over the molecular configurations of the dopants and electronic interactions with the π system.[58,59]

Therefore, in this review article, we will summarize recent key progress in the study of ORR electrocatalysis based on graphene-supported metal nanoparticles, where graphene may simply serve as a structural support for nanoparticle dispersion (following section), or more importantly, impact the electronic interactions of the metal nanoparticles with reaction species and hence the ORR performance (3rd section). We also discuss the latest breakthroughs of heteroatom-doped graphene as metal-free electrocatalysts for ORR (4th section) to highlight the diverse roles that graphene derivatives play in ORR electrocatalysis. Finally, we include a perspective (5th section) on the development of nontraditional ORR catalysts in light of the few and yet promising examples of MoS_2 for electrocatalytic oxygen reduction.[60–63]

GRAPHENE AS SUPPORTING SUBSTRATES

Carbon black (CB) is the most commonly used support material for nanoparticle catalysts.[48,49] However, there are several issues that limit the activity and durability of the catalysts, including: (i) the presence of organosulphur impurities; (ii) deep micropores or recesses which trap the catalyst nanoparticles making them inaccessible to reactants, thus leading to reduced catalytic activity; and (iii) thermochemical instability.[49] Therefore, other support materials have been explored. Yet, supports such as mesoporous carbon,[39–41] carbon nanofibers (CNF),[42,43] and carbon nanotubes (CNTs)[37,38] have generally not shown remarkable improvement over carbon black,[64,65] whereas graphene/graphene oxide (GO)/GQDs have emerged as promising supports for ORR electrocatalysts.[44–47]

Indeed, much progress has been made with graphene-supported Pt nanoparticles, as platinum has long been the catalyst of choice for ORR.[44,66–74] For instance, Kou *et al.*[66] prepared Pt nanoparticles (average dia. 2.0 nm) supported on functionalized graphene sheets (Pt-FGSs), which exhibited a high surface area (600 m^2 g^{-1} by the Brunauer–Emmett–Teller method) and a mass activity that was *c.* 30% better than that of commercial Pt/C, along with improved stability as manifested in durability tests. This was attributed to the π sites and functional groups in FSGs that enhanced metal–support interaction, leading to enhanced resistance of the Pt nanoparticles against sintering and aggregation and consequent improved stability and durability.

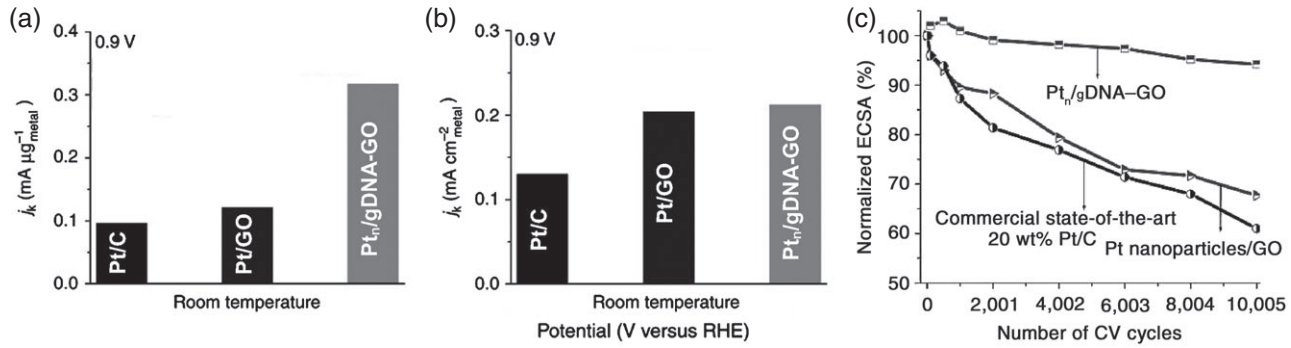

Figure 3. (a) Mass activity; (b) specific activity at 0.9 V versus RHE for different catalysts. Mass and specific activities are given as kinetic current densities (j_k) normalized in reference to the loading amount of metal and ECSA (ECSA from CO stripping), respectively; (c) comparison of decrease in ECSA for the catalysts. Reproduced with permission from ref. 71.

In another study, Chen and co-workers[44] prepared GQDs-supported Pt nanoparticles (Pt/GQD) as efficient ORR catalysts. TEM studies showed that Pt nanoparticles (average dia. 2.79 nm) were well dispersed and surrounded intimately by GQDs. Electrochemical studies showed that the ORR performance of Pt/GQD was markedly better than that of commercial Pt/C catalysts, as manifested by a more positive onset potential (E_{onset}, +1.05 V vs +0.98 V, both referenced to RHE) and higher kinetic current density (14.52 A m^{-2} vs 1.66 A m^{-2} at +0.90 V). Durability was also found significantly enhanced of the Pt/G catalysts over that of the Pt/C catalysts.

In other studies,[71,75] the graphene substrates are further functionalized or a second support is added to further enhance the activity and stability of the nanocomposite catalysts. For instance, Tiwari *et al.*[71] synthesized highly durable ORR electrocatalysts based on Pt_n nanoparticles (*c.* 1 nm in diameter) supported on double-stranded DNA-modified graphene oxide (Pt_n/gDNA-GO). CO-stripping voltammetric measurements showed that the electrochemical surface area (ECSA) of Pt_n/gDNA-GO (149.8 m^2 g^{-1}) was much larger than those of Pt/GO (without DNA modification, 59.1 m^2 g^{-1}) and commercial Pt/C (73.4 m^2 g^{-1}) – the latter nanoparticles were much larger, both around 2 to 3 nm in diameter. In ORR tests, the onset potential (E_{onset}) and half-wave potential ($E_{1/2}$) for the Pt_n/gDNA-GO were found to be at +1.01 V and +0.90 V, both markedly more positive than those of Pt/GO (+0.99 V, +0.83 V) and Pt/C (+0.95 V, +0.85 V). More significantly, the mass activity at +0.90 V for Pt_n/gDNA-GO was 317 A $g_{metal}{}^{-1}$, which was 3.3 and 2.6 times higher than that for the Pt/C and Pt/GO (Fig. 3(a)), and the area specific activity at +0.90 V for Pt_n/gDNA-GO was 1.63 and 1.03 times of that for Pt/C and Pt/GO, respectively (Fig. 3(b)). Accelerated degradation tests (ADT, Fig. 3(c)) also showed that the Pt_n/gDNA-GO catalysts exhibited the best stability among the series. The remarkable performance was attributed to the strong interactions between the nanosized platinum clusters and the DNA–GO composite, which manipulated the electronic structure of the platinum clusters.

In another study, Li *et al.*[75] inserted CB particles into Pt-loaded RGO, which effectively minimized the re-stacking of the RGO sheets and hence facilitated diffusion of oxygen through the catalyst layer, leading to a markedly enhanced ORR performance.

In comparison with Pt, Pd catalysts are usually a few times less active for ORR; yet Pd is more tolerant to CO poisoning and two/three times less expensive and more abundant than Pt,[76] making it especially suitable as cathode catalytic materials in, for instance, direct formic acid fuel cells,[77,78] direct alcohol fuel cells,[77,79,80] and polymer electrolyte membrane fuel cells.[79,80] Thus, research efforts have been focused primarily on enhancing the Pd activity by alloying with other elements, tuning the local chemical environment, and improving the interactions with the support materials.[81] Among those, loading Pd nanoparticles on graphene (or GO/GQDs) is an effective way to improve the ORR activity. In a theoretical work, Liu *et al.*[81] studied the impacts of graphene support on the electrocatalytic activity of Pd nanoparticles by first-principles calculations. They found that the binding energy of a Pd_{13} nanoparticle on a single vacancy graphene was as high as −6.10 eV due to hybridization between the Pd dsp states and the sp^2 dangling bonds at the graphene defect sites, prohibiting the sintering and segregation of the Pd nanoparticles. Such strong interaction between the Pd nanoparticles and graphene also led to a shift of the Pd d band center from −1.02 to −1.45 eV, and hence an improved ORR activity. Furthermore, the electrocatalytic activity may be further enhanced by the weakened adsorptions of OIs as the adsorption energies of O, OH, and OOH are reduced from −4.78, −4.38, −1.56 eV on the freestanding Pd_{13} nanoparticles to −4.57, −2.66, and −1.39 eV on the Pd_{13}/single vacancy graphene composites.

In an experimental study, Seo *et al.*[82] prepared graphene nanosheets (GNS) supported Pd nanoparticles (Pd/GNS) which showed high ORR activity in alkaline media, compared with Pt/GNS (Fig. 4). TEM studies showed that GNSs exhibited a sheet-like morphology and Pd or Pt nanoparticles were well dispersed on the GNS surface (average dia. 1.80 nm for Pd and 1.87 nm for Pt). Electrochemical studies in oxygen-saturated 0.1 mol L^{-1} NaOH (Fig. 5) showed that for Pd/GNS, E_{onset} = +1.05 V and $E_{1/2}$ = +0.90 V, more positive than those for Pt/GNS (E_{onset} = +1.00 and $E_{1/2}$ = +0.85 V). The number (n) of electron transfer in ORR is also higher for Pd/GNS (3.97) than for Pt/GNS (3.81). Furthermore, the Pd/GNS catalysts showed good durability, retaining more than 90% of the initial activity after 100 cycles, due to the strong interactions between Pd and GNSs.

In another study, Truong-Phuoc *et al.*[83] prepared few-layered graphene-supported palladium (Pd/FLG, dia. 3–20 nm), which showed a markedly better ORR catalytic performance than commercial Pd/C and Pt/C. For instance, E_{onset} and $E_{1/2}$ are both ~50 mV more positive than those of Pd/C and Pt/C (Fig. 6(a)). Furthermore, the specific activity (j_s) for Pd/FLG is also much higher (Fig. 6(b)). For instance, j_s at +0.90 V was about 3.9 mA cm^{-2} for Pd/FLG, much higher than 2.6 mA cm^{-2} and 2.8 mA cm^{-2} for Pt/C and Pd/C, respectively. What is more, from Fig. 6(c) and (d) it can be seen that Pd/FLG exhibited excellent stability in long-term operation, compared with Pd/C and Pt/C, where the ECSA remained almost

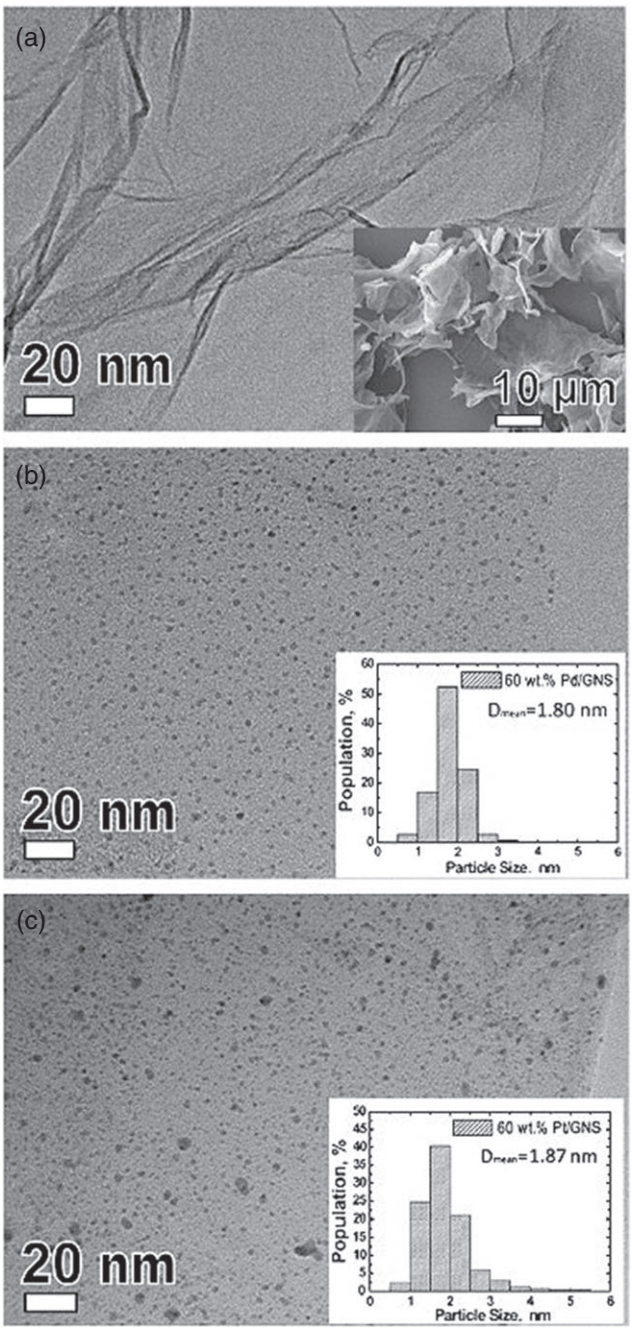

Figure 4. TEM images of (a) GNS, (b) Pd/GNS and (c) Pt/GNS, with corresponding histograms of particle sizes. The inset to Fig. 4(a) shows an image of a GNS obtained by scanning electron microscopy (SEM). Insets to panels (b) and (c) are the corresponding core size histograms. Reproduced with permission from ref. 82.

unchanged after 2500 cycles and j_s only dropped by 2% for Pd/FLG, while 35% and 20% for Pt/C and Pd/C, respectively. In addition, Pd/FLG also showed better methanol tolerance than Pd/C and Pt/C. These were accounted for by the strong interactions between the Pd nanoparticles and the graphene sheets, leading to electron transfer or charge redistribution through the hybridization of Pd and FLG electronic states, and lattice strain of the first few layers of Pd atoms grown on FLG.[84,85]

Unlike platinum-group metals, bulk gold has attracted little attention in electrocatalysis mainly due to its poor catalytic performance. However, when the dimensions of the gold catalysts are diminished to the nanoscale, the properties of the material exhibit a dramatic deviation from those of bulk Au.[86,87] In fact, a series of studies have been carried out to examine the ORR activity of gold nanoparticles.[88–90] Of these, graphene (including GO and GQDs) has been used as support materials to help disperse gold nanostructures and enhance the ORR performance.[89–93] For instance, Govindhan *et al.*[94] electrochemically deposited Au nanoparticles (average diameter 6.8 nm) on reduced GO (Au/RGO) that was cast onto a glassy carbon electrode (GCE) surface. Electrochemical measurements clearly show a much enhanced ORR activity of the Au/RGO catalysts over that with gold nanoparticles alone in both 0.1 mol L^{-1} H_2SO_4 and KOH solutions.

In another study, Wang, *et al.*[95] deposited smaller gold nanoparticles (3–5 nm in diameter) on sulfhydryl-functionalized graphene oxide (Au–GOSH). Electrochemical measurements demonstrated that the Au–GOSH hybrid exhibited a markedly better ORR performance, with a more positive onset potential and higher reduction current, than bulk Au electrode, gold nanoparticles alone on GCE, and Au/RGO composite in another study.[92] From the Tafel plots, one can tell that Au–GOSH exhibited a larger exchange current density than individual Au nanoparticles, indicating that the improved activity resulted from the synergetic effect of gold nanoparticles and graphene. Moreover, durability tests showed the Au–GOSH hybrid exhibited excellent stability during ORR measurements with a constant current for 10 h.

Yin *et al.*[93] prepared even smaller Au nanoparticles (dia. 1.8 ± 0.2 nm) that were surfactant-free and deposited on RGO surfaces (Au/RGO) by the freeze-drying method. Voltammetric measurements demonstrated that the n value for ORR at Au/RGO was 3.6 to 3.7 in the potential range −0.8 to −0.3 V (vs Ag/AgCl), with $E_{onset} = -0.1$ V vs. Ag/AgCl (or *c.* +0.87 V vs RHE). Whereas the limiting current was apparently lower than that of commercial Pt/C, the Au/RGO hybrids exhibited much improved long-term durability where the onset potential degraded by only 33 mV compared with 82 mV for commercial Pt/C after continuous operation for 20 h. The ORR performance was attributed to three factors: the diminished Au particle size led to a decreased activation energy for the dissociation of absorbed oxygen molecules; the absence of capping ligands facilitated charge transfer at the metal–carbon interface; and the synergetic coupling between Au particles and RGO lowered the dissociation activation energy of oxygen by enhanced charge transfer between metal and oxygen as well as the reduced energy barrier for the rate-determining step.

Silver has also been explored as a possible ORR catalyst.[96,97] In a recent study, Lim *et al.*[98] prepared highly dispersed Ag nanoparticles (dia. ∼10 nm, Fig. 7(b)) on RGO (Fig. 7(a)) at a high Ag loading of 60 wt%, and examined the ORR activity in alkaline media, compared with commercial carbon-supported Ag catalysts (60 wt% Ag/C from Premetek, Fig. 7(c)). Lead underpotential deposition (UPD) showed that the ECSA was 1.9 cm^2 for Ag/RGO and only 0.2 cm^2 for Ag/C. ORR tests were then carried out in an oxygen-saturated 0.1 mol L^{-1} NaOH solution where Ag/RGO exhibited a much higher ORR activity than Ag/C, with a more positive E_{onset} (+0.01 V vs. Hg/HgO (1 mol L^{-1} KOH)) and $E_{1/2}$ (around −0.23 V vs. Hg/HgO (1 mol L^{-1} KOH)). Furthermore, the mass-specific kinetic current density of the Ag/RGO catalysts at −0.23 V (vs. Hg/HgO (1 mol L^{-1} KOH)) was calculated to be 10 mA mg^{-1}, four times higher than that for Ag/C. In addition, the n value was 3.9 for Ag/RGO within the potential range of +0.65 to +0.80 V (vs. Hg/HgO (1 mol L^{-1} KOH)), much larger than that (<2.5) for Ag/C. This indicates that oxygen was reduced at Ag/C through

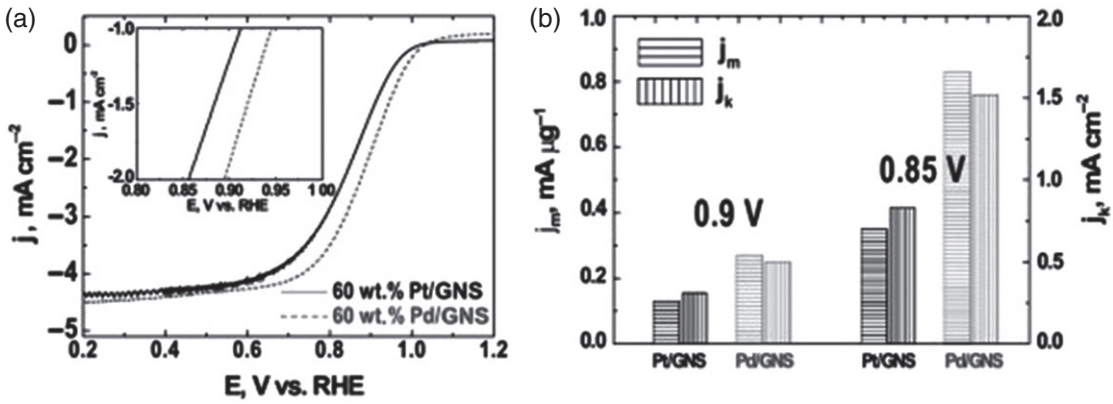

Figure 5. (a) Comparison of the polarization curves for the ORR in an O_2-saturated 0.1 mol L^{-1} NaOH solution with a sweep rate of 10 mV s^{-1} at room temperature; rotating speed: 1600 rpm. Inset is the zoom-in of the voltammetric profiles within the potential range of 0.85 to 1.0 V. (b) Bar plots of the ORR mass and surface area normalized activities (j_m and j_k) at 0.9 and 0.85 V vs. RHE. Reproduced with permission from ref. 82.

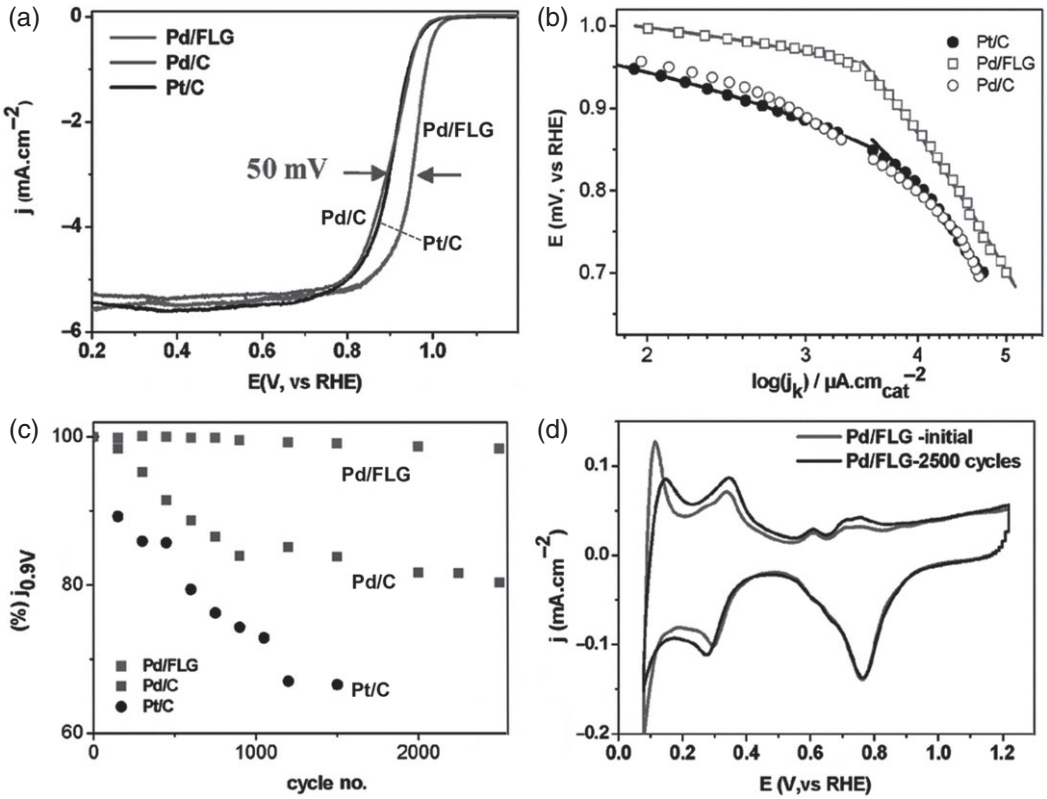

Figure 6. ORR performance of Pd/FLG (vs. Pt/C and Pd/C): (a) polarization curves, (b) Tafel plots, (c) Pd/FLG, Pd/C and Pt/C current density drops at +0.9 V with cycle number, (d) ECSA measurement–CV curves of Pd/FLG before and after 2500 cycles, RHE = reversible hydrogen electrode. Reproduced with permission from ref. 83.

both the 2- and 4-electron reduction pathways, while at Ag/RGO ORR predominantly proceeded by the 4-electron reduction pathway under alkaline conditions.

Lee *et al.*[99] prepared silver nanoparticles supported on dithiol-functionalized GO sheets (GO-S$(CH_2)_x$SH with $x = 2$, 3, and 4). The size of the Ag nanoparticles in the resulting GO-C_x-Ag hybrids increased with decreasing ligand length, 3.0 nm at $x = 2$, 5.6 nm at $x = 3$, and 8.6 nm $x = 4$. At $x = 0$ (the composite was denoted as GO-Ag), however, the Ag nanoparticles were much larger at around 20 nm. The corresponding ECSA decreased accordingly at 72, 63, 53, and 45 m^2 g^{-1}, respectively. Electrochemical studies showed that the GO–C_2–Ag sample exhibited the best ORR activity among the series with the most positive E_{onset} (−0.11 V vs. Ag/AgCl), highest kinetic current density, and largest n value (3.8 to 4 within the potential range of −1.2 to −0.6 V vs Ag/AgCl). However, it remained unclear whether the enhanced performance was due to the diminishing nanoparticle core size and/or to the short surface capping ligands.

Graphene derivatives have also been exploited to support other metal/alloy/oxide nanoparticles for ORR electrocatalysis. For instance, enhanced ORR activity has been observed with copper oxide nanoparticles grown on nitrogen-doped RGO surface, in comparison to N-RGO alone or CuO/GO composites.[100] Studies have also been carried out with nanocomposites based on

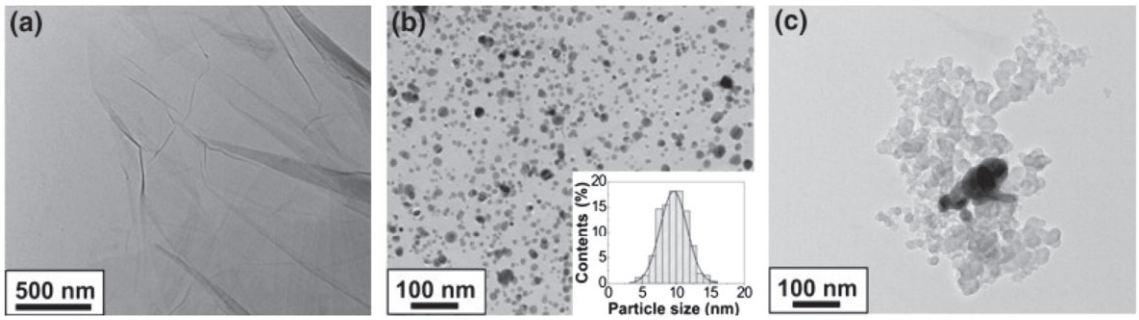

Figure 7. TEM images of the prepared (a) GO, (b) 60 wt% Ag/RGO, (c) 60 wt% Ag/C (Premetek) catalysts. Reproduced with permission from ref. 98.

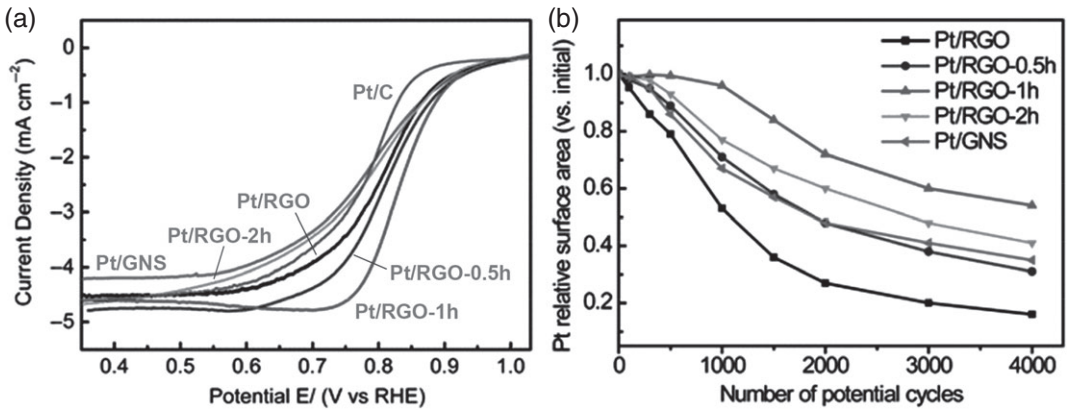

Figure 8. (a) Current–potential curves for ORR of Pt/RGO, Pt/RGO-0.5 h, Pt/RGO-1 h, Pt/RGO-2 h, Pt/GNS, and Pt/C catalysts. (b) Changes in the ECSA of catalysts with increasing number of potential cycles. Reproduced with permission from ref. 110.

graphene-supported metal alloy nanoparticles[70,101–105] or metal oxide nanoparticles such as Co_3O_4[46] and Co/CoO.[106] In these prior studies, the ORR results are interpreted within the context where graphene derivatives primarily serve as a structural support to enhance dispersion and minimize aggregation of the nanoparticle catalysts. However, further studies suggest that graphene might play a far more active role in manipulating the ORR activity by electronic interactions with the metal nanoparticles as well as by heteroatom doping that impacts the bonding interactions with oxygen species. These will be summarized below.

ELECTRONIC INTERACTIONS BETWEEN GRAPHENE AND NANOPARTICLE CATALYSTS

In the above studies, oxygen-containing functional groups of graphene derivatives have been proposed to improve the metal–graphene interactions, stabilize the metal nanoparticles, prevent $\pi - \pi$ stacking between the graphene sheets, and therefore enhance the ORR activity of the metal nanoparticles. Note that in some previous reports[107–109] it was claimed that the higher the graphitization degree of the carbon supports, the higher the electrochemical stability for carbon supported Pt catalysts. Therefore, several studies[45,110] have been conducted to investigate the relationship between the ORR performance and the amount of oxygenated groups or defects on the graphene surface.

For instance, He *et al.*[110] found that by having a certain amount of oxygen-containing groups on the RGO surface the ORR performance of the Pt/RGO catalysts could be greatly improved. This suggests bifunctional effects of RGO on the activity and stability of Pt catalysts by compromising the degree of graphitization and the amount of oxygen-containing groups on the RGO surface. Experimentally, the degree of deoxidization of GO was manipulated by thermal treatment of Pt/RGO nanocomposites at 300 °C in a H_2 atmosphere for 0.5, 1, and 2 h, respectively, and the final products were named as Pt/RGO-0.5 h, Pt/RGO-1 h, and Pt/RGO-2 h. Raman and XPS measurements showed the formation of increasingly graphitic carbons after the heat treatment, leading to diminishment of the charge transfer resistance (R_{CT}), as manifested in electrochemical impedance measurements. The results indicate that the oxygen-containing groups did play an important role in metal-support interactions. Voltammetric measurements in Fig. 8(a) showed that the mass activity for Pt/RGO-1 h was 9.2 mA mg^{-1}, which is 1.3 and 1.5 times those of the Pt/RGO (7.3 mA mg^{-1}) and the Pt/GNS (6.3 mA mg^{-1}), respectively. This enhancement was ascribed to the increase of the RGO conductivity as well as the well-dispersed Pt nanoparticles on the RGO surface. However, when the heating time increased to 2 h, the catalytic activity of Pt/RGO decreased, probably due to nanoparticle aggregation. The stability of the Pt/RGO samples as ORR catalysts were also evaluated. As shown in Fig. 8(b), it is evident that Pt/RGO-1 h was the most stable sample among the series. After 4000 cycles of potential sweeps, 54.0% of the initial ECSA was retained, much higher than those of others.

In another study, Song *et al.*[45] identified an optimal concentration of the structural defects within GQDs for maximal ORR activity of Pt/GQD nanocomposites. The GQD structural defects were manipulated by hydrothermal treatment at controlled temperatures (140 to 200 °C) for different periods of time (3, 6, and 12 h). TEM measurements (Fig. 9) showed that the sizes of the Pt nanoparticles were in the narrow range 2.5 to 3.5 nm in diameter

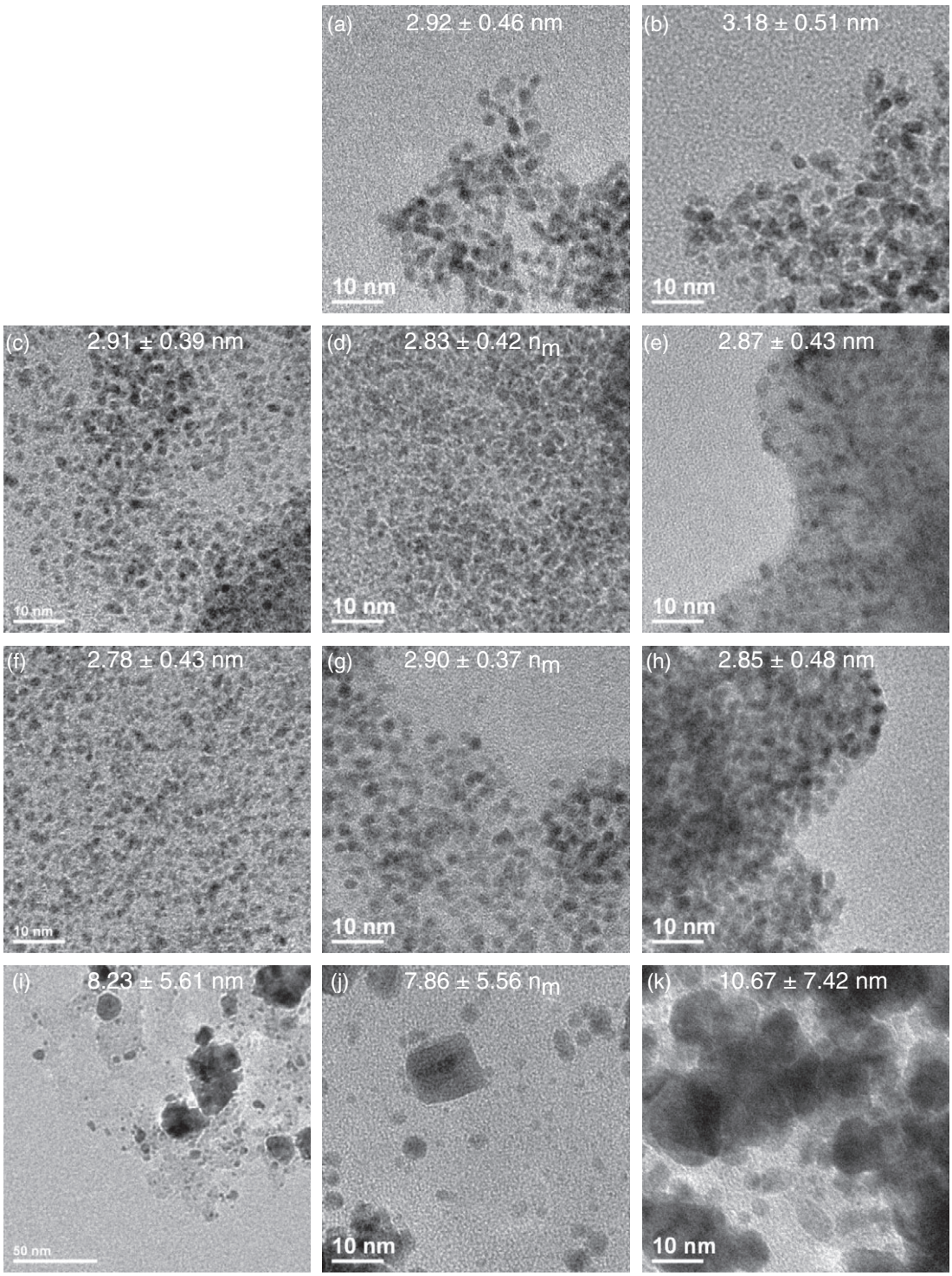

Figure 9. Representative TEM micrographs of GQD-supported Pt nanoparticles prepared by hydrothermal treatment at various temperatures for different periods of time: (A) 140 °C, 6 h; (B) 140 °C, 12 h; (C) 160 °C, 3 h; (D) 160 °C, 6 h; (E) 160 °C, 12 h; (F) 180 °C, 3 h; (G) 180 °C, 6 h; (H) 180 °C, 12 h; (I) 200 °C, 3 h; (J) 200 °C, 6 h; and (K) 200 °C, 12 h. Scale bars are all 10 nm except for panel (I) where it is 50 nm. Reproduced with permission from ref. 45.

and averaged below 3.0 nm when the hydrothermal temperatures were kept within the range 140 to 180 °C, but markedly larger at 8–12 nm in diameter when the temperature went up to 200 °C. This was because hydrothermal treatment at high temperatures (200 °C) decreased the GQD defect concentration, rendering it difficult to effectively passivate the Pt nanoparticles and consequently the Pt particle size increased.[111] In fact, FTIR measurements showed that after hydrothermal treatment the vibrational bands of oxygen-containing groups like O–H, C=O, and C–O–C groups diminished significantly or even disappeared, and the C=C stretches exhibited an apparent red-shift. This was accounted for by the (partial) removal of the oxygen-containing groups and the restoration and hence growth of the sp^2 carbon domains in GQDs. This is consistent with results from

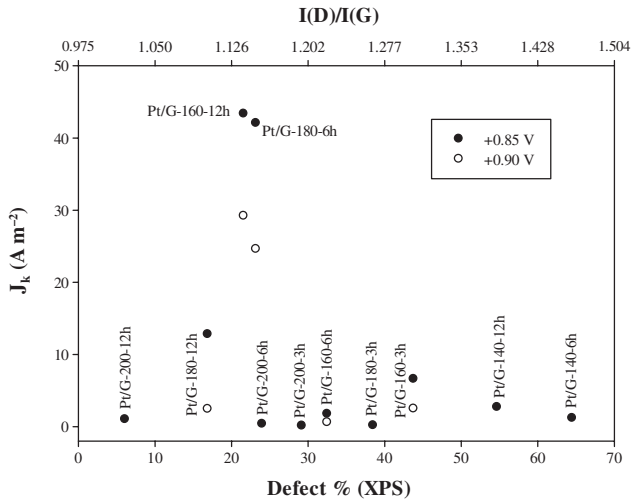

Figure 10. Variation of the ORR kinetic current density at +0.85 (solid circles) and +0.90 V (empty circles) with GQD structural defects manifested as the defect concentrations from XPS measurements and I(D)/I(G) ratio in Raman spectroscopic measurements. Reproduced with permission from ref. 45.

Raman measurements where the ratio (*I*(D)/*I*(G)) of the D and G band intensity decreases with the increase of the heating temperature and treatment time. That is, the GQDs defect concentration could be readily controlled by varying experimental conditions.

XPS analysis showed that the concentration of non-sp^2 carbons (collectively defined as defects) decreased markedly with increasing hydrothermal temperature and reaction time, and an approximately linear relationship was observed between the atomic ratio of defective carbons to total carbons and the *I*(D)/*I*(G) ratio, suggesting direct correlation between the two measurements. Furthermore, the Pt/G-160-12 h (160 °C for 12 h) and Pt/G-180-6 h (180 °C for 6 h) samples were found to exhibit the lowest binding energies of Pt4f electrons among the series, signifying minimum charge transfer from Pt to GQDs in these two samples. Interestingly, these two samples also exhibited the best electrocatalytic performance in ORR, as manifested in RRDE voltammetric measurements. As depicted in Fig. 10, the ORR activity exhibited a volcano-shaped variation with the GQD defect concentration (quantified by XPS and Raman measurements), and the Pt/G-180-6 h and Pt/G-160-12 h samples stood out as the best among the series. This can be ascribed to the intimate interactions between the Pt nanoparticles and the GQDs, leading to the deliberate manipulation of the d-band center of the Pt nanoparticles and hence the charge transfer dynamics of the oxygen reduction.[8,112]

In a recent theoretical study,[113] it was shown that strong binding between small metal nanoclusters and graphene can be achieved by growing metal nanoclusters on both sides of the graphene sheet where the nanoclusters may even penetrate the plane. This leads to even higher thermodynamic stability than metal nanoclusters grown only on one side of a graphene support. More importantly, higher catalytic activity may arise, because a new band gap is introduced into the graphene plane by the *in situ* formed defects, providing a possible tool to further tune the electronic properties of graphene. The electrocatalytic activity may also be improved because of the formation of a Mott–Schottky contact at the metal–carbon interface.[114] Inspired by this, Lv *et al.*[115] synthesized a graphene-based nanocomposite with cobalt nanocrystals anchored through nitrogen-doped graphene planes (CoNPs@NG), which showed superb electrocatalytic activity and stability for ORR, outperforming even state-of-the-art Pt/C catalysts. The CoNPs@NG hybrids (Co 5 wt%) were prepared through a simple one-step pyrolysis method by using $CoCl_2$, glucose, and dicyandiamide as precursors. XRD measurements showed three peaks that were consistent with the (111), (200), and (220) planes of metallic Co (standard PDF card 15–0806), but no peaks corresponding to graphene oxide, cobalt oxides, carbides, or nitrides. From TEM measurements (Fig. 11), Co nanoparticles can be clearly identified with an average diameter of 15 nm, and selected area electron diffraction (SAED, Fig. 11(b) inset) further confirms the formation of metallic Co nanoparticles. The ORR activity of CoNPs@NG was then investigated with linear sweep voltammetry (LSV). From Fig. 12(a), E_{onset} and $E_{1/2}$ for ORR in an alkaline solution can be estimated to be at +1.06 and +1.01 V vs. RHE, respectively, which are more positive than those for bare NG (+0.90 and +0.81 V), Pt/C (+0.98 and +0.87 V), and other nanoparticle/graphene based electrocatalysts.[46,106,116–119] Furthermore, as shown in Fig. 12(b) and (e), the numbers of electron transfer for CoNPs@NG within the potential range of +0.20 to +1.00 V were very close to 4 (from 3.80 to 3.99), and the Tafel slope of 85 mV/dec was close to that for commercial Pt/C, indicating favorable ORR kinetics for a 4-electron process on the CoNPs@NG

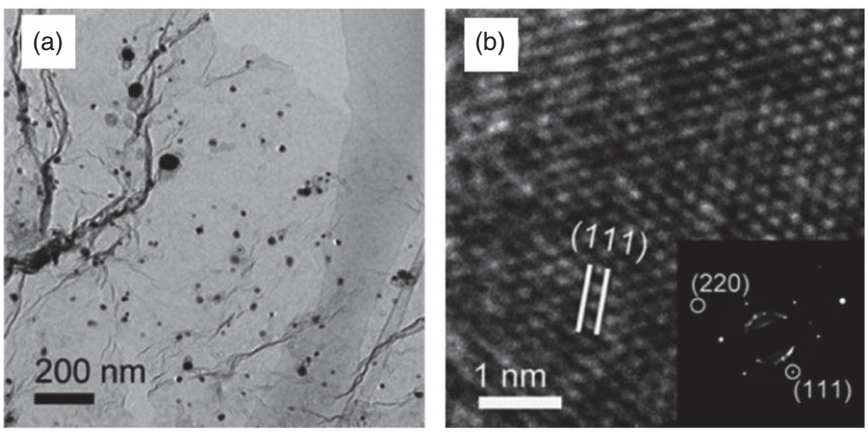

Figure 11. TEM image (a), and HRTEM (b) image of CoNPs@NG. Inset to (b) is the selected area electron diffraction pattern. Reproduced with permission from ref. 115.

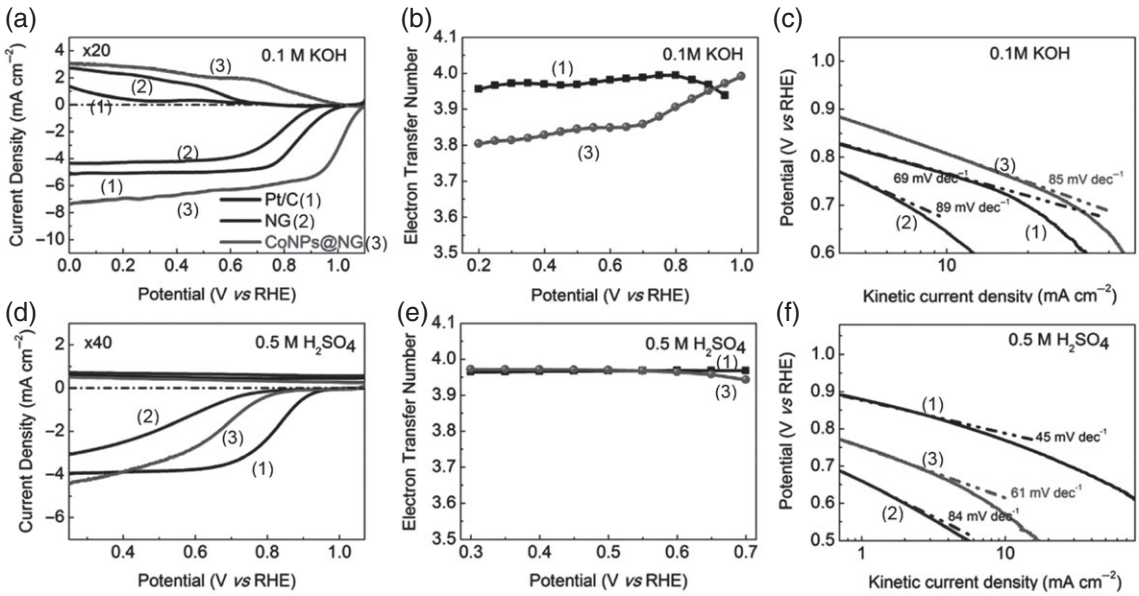

Figure 12. Electrocatalytic activity of various samples in alkaline (a)–(c) and acid (d)–(f) electrolyte. Rotating ring-disk electrode voltammograms (a),(d), the electron transfer number (b),(e), and corresponding tafel slopes (c),(f) of Pt/C, bare NG, and CoNPs@NG. All measurements were conducted on glassy carbon electrodes at 1600 rpm in O_2-saturated electrolytes with a sweep rate of 10 mV s^{-1}. Reproduced with permission from ref. 115.

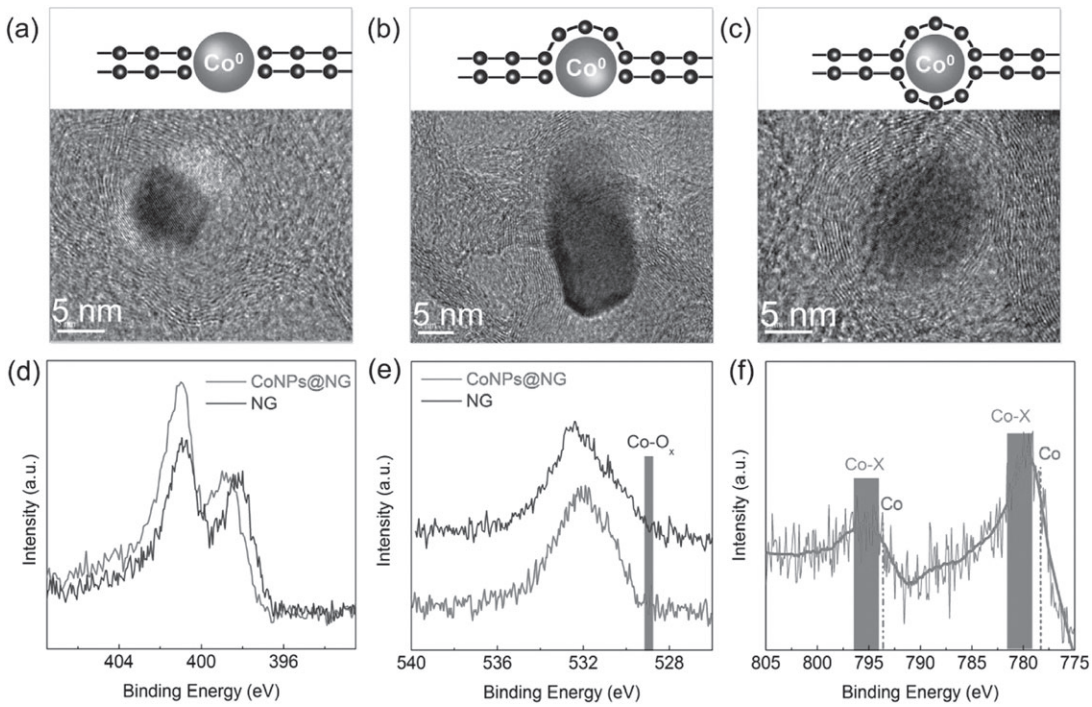

Figure 13. HRTEM images of CoNPs@NG with the Co NPs uncovered (a), partly covered (b), and completely covered (c) by graphene layers. (d) High resolution XPS N1s spectra of NG and CoNPs@NG. (e) High resolution XPS O1s spectra of NG and CoNPs@NG. (f) High resolution XPS Co 2p spectrum of CoNPs@NG with both metallic Co and Co-X bonds (X might be C, N, or O). Reproduced with permission from ref. 115.

catalysts, likely due to the promoting effect of Co (Fig. 12(d), (e), and (f)).

To unravel the mechanistic origin, further studies were conducted, and three types of Co NPs were observed: uncovered, partly covered, and completely covered (Fig. 13(a), (b), and (c)). XPS measurements (Fig. 13(d), (e), and (f)) showed that the cobalt was mostly metallic with a small amount of Co–N species but no Co–O, signifying that the Co NPs anchored through the graphene plane via the Co–N bond, and more importantly, the involvement of Co in the NG structure also resulted in an increased amount of graphitic N atoms (Fig. 13(d)), leading to the formation of highly active sites for ORR.

In a control test, the ORR activity of CoNPs@NG was found to diminish markedly after the addition of KSCN into the electrolyte solution (Fig. 14). This further confirmed that the Co–N–C compounds (which would be readily poisoned by CN^- or SCN^-) at the Co NPs-NG interface were largely responsible for the activation of oxygen and the eventual ORR activity. Interestingly,

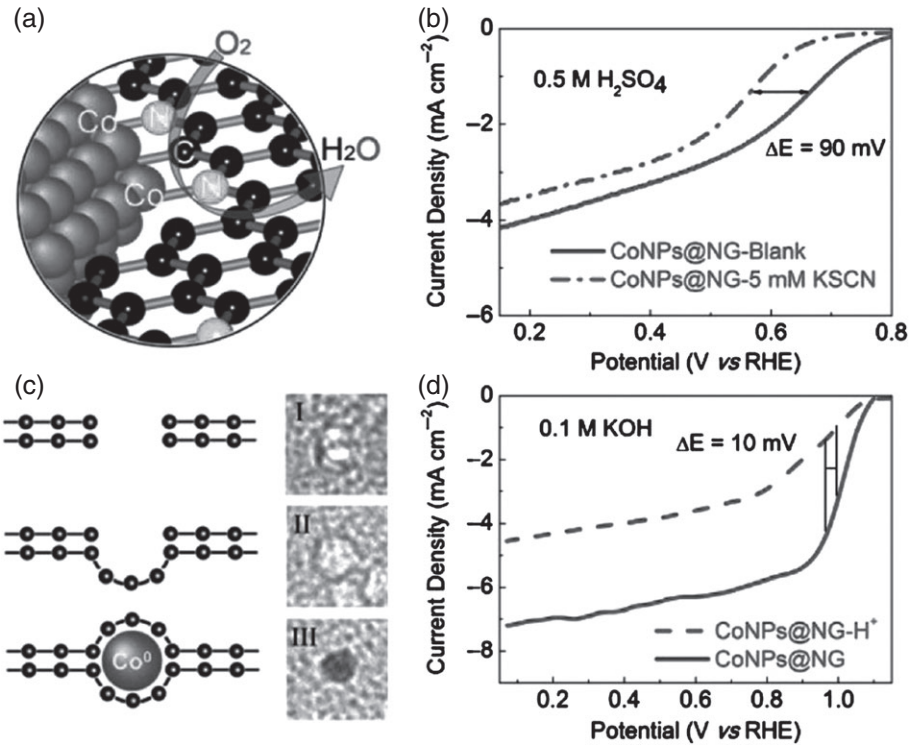

Figure 14. Effect of the structure on the ORR activity. (a) Scheme of the active site at the interface of Co NPs and NG. Effect of SCN^- ions on ORR activity of CoNPs@NG (b) catalyst was tested in 0.5 mol L^{-1} H_2SO_4. The final concentration of SCN^- was 5 mmol L^{-1}. (c) Cartoon schemes and TEM images of typical nanostructures in CoNP@NG-H^+ (obtained by etching CoNPs@NG sample in 7.5 mol L^{-1} HNO_3 for 24 h at room temperature). (b) LSV curves of CoNPs@NG and CoNP@NG-H^+ tested in alkaline electrolyte. Reproduced with permission from ref. 115.

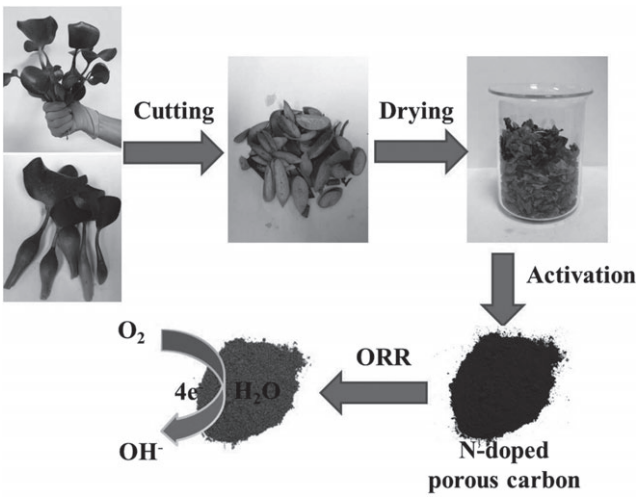

Figure 15. Schematic of the synthesis of N self-doped porous carbon from water hyacinth. Reproduced with permission from ref. 133.

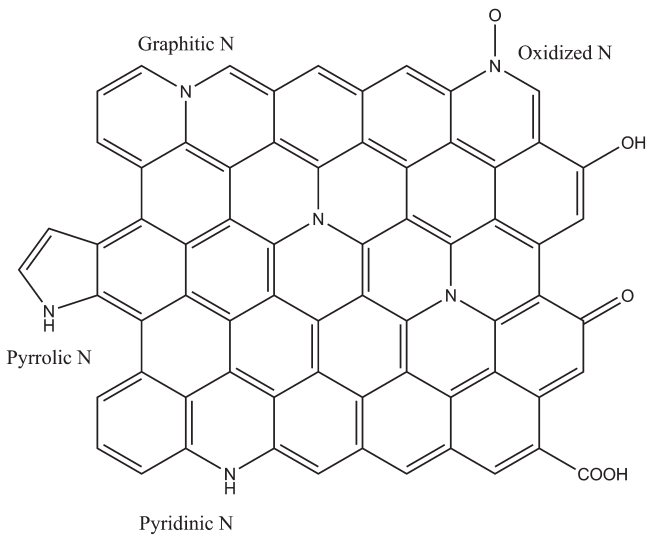

Figure 16. Schematic representation of the different N bonding configurations.

the SCN^- poisoned CoNPs@NG still exhibited better ORR performance than bare NG, suggesting additional contributions from electrocatalytically active sites other than the Co–N complexes. In addition, even after partial removal of Co from CoNPs@NG, the sample remained highly active for ORR with no obvious shift of the onset and half-wave potentials, but only a decreased limiting current density. This was probably due to electron redistribution among the tightly bonded Co, N, and C that introduced a new band gap into graphene and made graphene domains adjacent to Co NPs more active for ORR. However, partial removal of Co nanoparticles also led to decreased electric conductivity and hence decreased limiting current density.

Taken together, these results suggest that ORR at CoNPs@NG composites mostly involved two types of active sites, the N-doped graphene domains adjacent to Co as the main sites for oxygen activation, and the metallic Co NPs for high electric conductivity and high limiting currents. The stability of CoNPs@NG was also evaluated in both alkaline and acidic solutions by choronoamperometric measurements. The activity was reduced by less than 10%

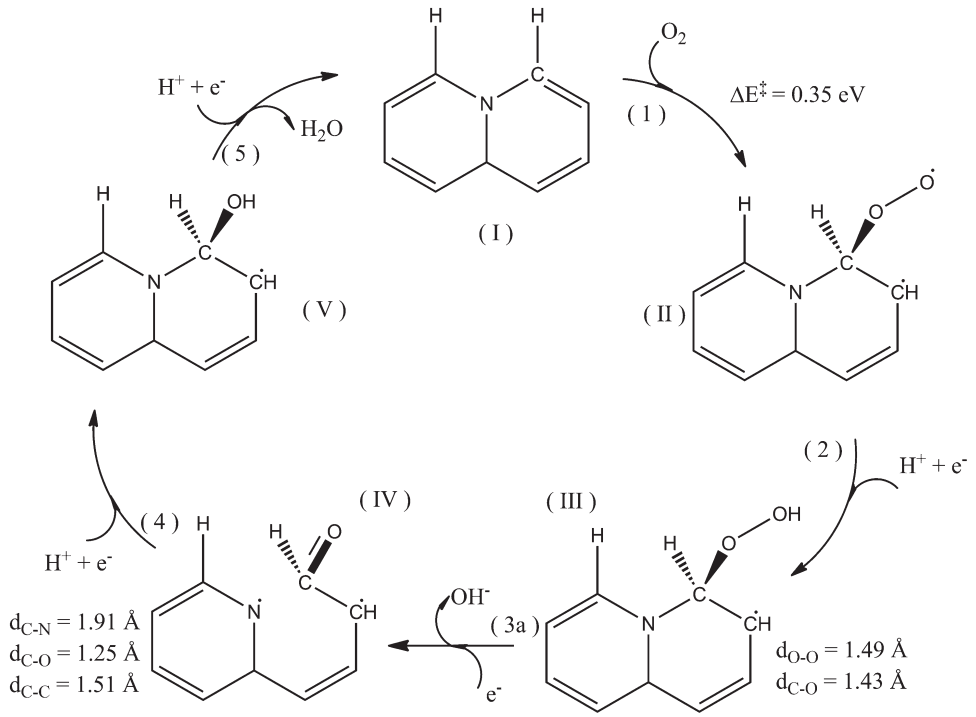

Figure 17. Proposed ORR mechanism on N-doped graphene nanoribbons. Reproduced with permission from ref. 141.

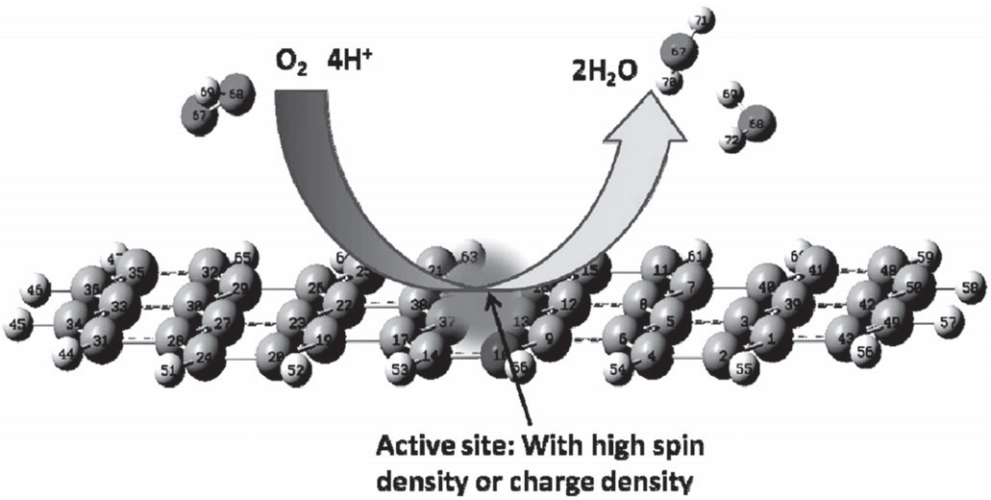

Figure 18. Schematic representation of the active sites in doped carbon materials. Reproduced with permission from ref. 151.

for the CoNPs@NG catalysts either in alkaline or acidic solution after 30 000 s, whereas both the Pt/C and the CoNPs + NG catalysts lost about 50% of their ORR activity. All these results indicate the superior ORR electrocatalytic activity of the CoNPs@NG hybrids.

DOPED GRAPHENE FOR METAL-FREE ELECTROCATALYSIS

Besides serving as supporting substrates for nanoparticle catalysts, graphene-based materials have also been found to act as metal-free electrocatalysts with remarkable ORR activity and durability when doped with heteroatoms such as N, B, S, and Se.[53,54,120] The originally ORR-inert π electrons may be activated via selective doping so that O_2 molecules can be efficiently reduced on the carbon surface.[56,57] Several methods are commonly used to prepare N-doped carbons. One of these is chemical vapor deposition using N-,[55,121] B-,[122,123] or S-[124] containing precursors. However, this is not applicable for large-scale production due to special synthetic instruments and demanding experimental conditions.

One convenient and inexpensive route is based on hydrothermal treatment at controlled temperatures using C- and N-containing precursors with appropriate activation reagents. For example, Liu *et al.*[125] prepared N-doped porous carbons with a specific surface area up to 1000 $m^2 g^{-1}$ by hydrothermal treatment of glucose and dicyandiamide with $ZnCl_2$ as an activation reagent. The samples exhibited a remarkable ORR activity in alkaline media, with E_{onset} as positive as +0.96 V, high selectivity of 4-electron reduction, and superior methanol tolerance, a performance that was comparable with that of state-of-the-art Pt/C catalysts. In fact, N-doped carbons have also been prepared by direct

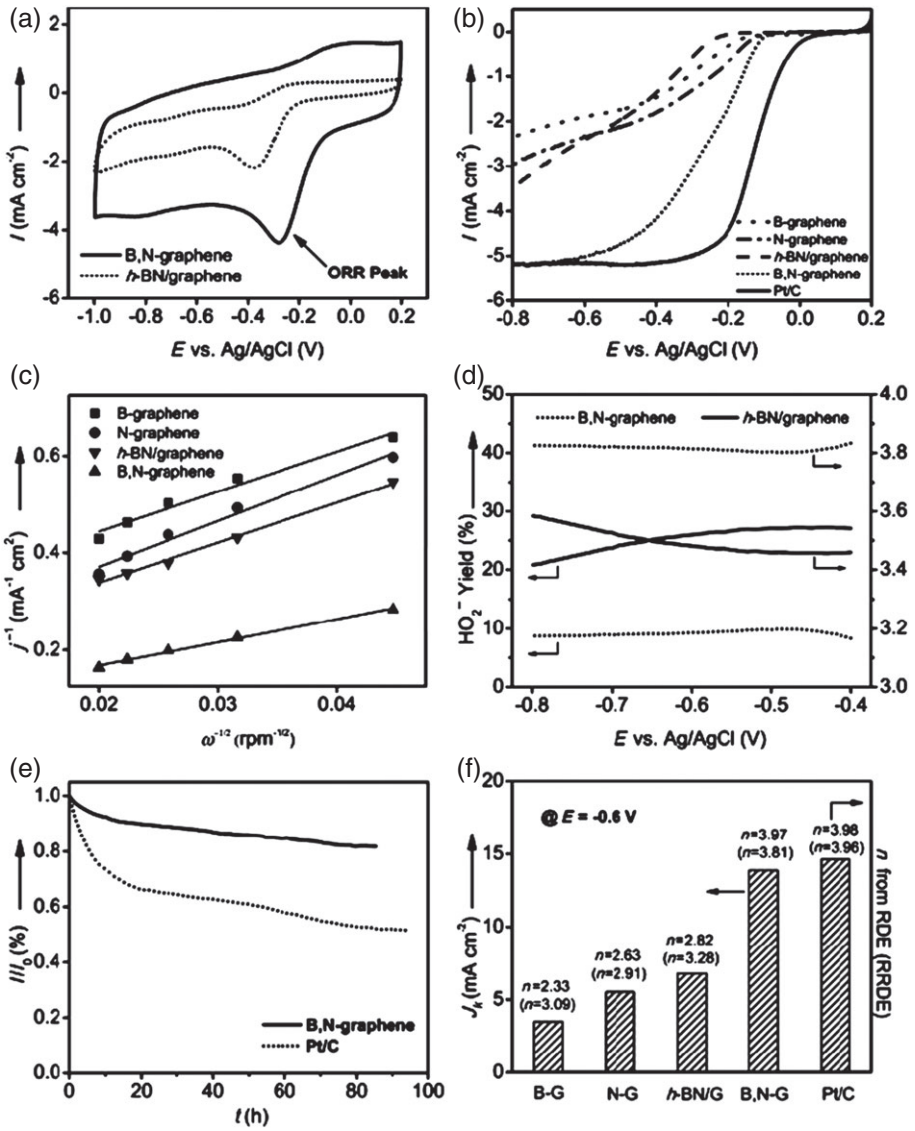

Figure 19. (a) Cyclic voltammograms of ORR on B,N-graphene and the *h*-BN/graphene hybrid in an O_2-saturated 0.1 mol L^{-1} solution of KOH (scan rate: 100 mV s^{-1}). (b) LSV of various electrocatalysts on a RDE (1500 rpm) in an O_2-saturated 0.1 mol L^{-1} solution of KOH (scan rate: 10 mV s^{-1}). (c) K–L plots at −0.6 V for various catalysts on the basis of the RDE data. (d) Extent of HO_2^- production and the corresponding electron-transfer number of B,N-graphene and *h*-BN/graphene, as based on the RRDE data. (e) Chronoamperometric response of B,N-graphene and Pt/C at −0.3 V in an O_2-saturated 0.1 mol L^{-1} solution of KOH. (f) Summary of the kinetic limiting current density and the electron-transfer number on the basis of the RDE data and the RRDE data (values in parentheses) on various catalysts (G stands for graphene in the *x*-axis labels). Reproduced with permission from ref. 153.

pyrolysis of a wide variety of nitrogen-rich precursors, such as cyanamide,[126] ethylenediamine,[127] hexamethylenediamine,[128] melamine foam,[129] and polymer frameworks.[130,131] More recently, direct pyrolysis of environmentally hazardous materials has also been used to prepare nitrogen self-doped porous carbons, such as surplus sludge[132] (a toxic byproduct from microbial wastewater treatments) and water hyacinth (Fig. 15),[133] and exhibited apparent ORR activities that was comparable to or even better than leading literature results.

Whereas direct pyrolysis is currently the most popular method, active N-species may be inevitably lost during the high temperature calcination, and it is difficult to control the porosity. Thus, heat treatment at moderate temperatures of graphene-based materials with N-containing species is an effective alternative. For instance, Wang and coworkers[134] covalently functionalized graphene nanoribbons with nitrogen species via high-power electrical joule heating in ammonia gas, where the carbon–nitrogen bonds were found to form mostly at highly reactive graphene edges. Other post-treatment methods include annealing GO in the presence of melamine,[135] heat-treatment of graphene with NH_3,[53] and thermal annealing GO with 5-aminotetrazole monohydrate.[136] To further decrease the temperature for thermal treatment, Wu *et al.*[137] hydrothermally treated GO with urea, and Zhang *et al.*[138] utilized wet-chemical reduction between GO and dicyandiamide to prepare N-doped graphene. In general, these post-synthesis methods usually yield doped carbon materials with a low nitrogen concentration possibly due to the difficulty of incorporating heteroatoms into the pre-existing graphitic skeletons at low temperatures.

In these studies, it has been found that the type of nitrogen dopants plays a critical role in determining the ORR performance. There are four typical configurations for nitrogen dopants: pyridinic, pyrrollic, graphtic, and pyridinic N in oxidized form (also

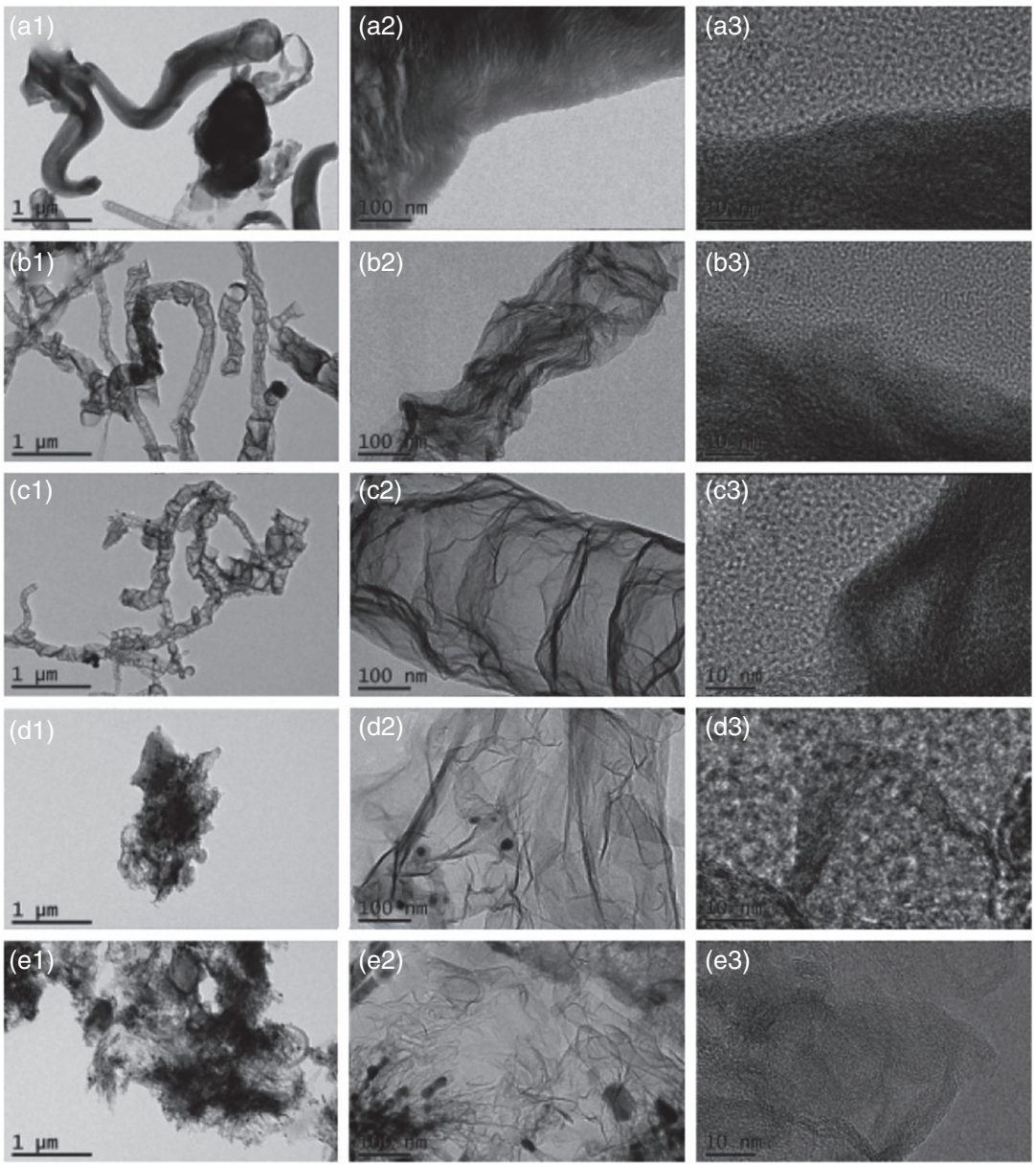

Figure 20. TEM images of the prepared catalysts for (a) NDC, (b) PNDC-5, (c) PNDC-10, (d) PNDC-15, and (e) PNDC-20, and are indicated by 1 to 3 according to the magnifications (1. × 6000; 2. × 40000; 3. × 400000). 'x3' images (x = a to e) are captured at the edge of the catalysts. Reproduced with permission from ref. 154.

called quaternary N), as depicted in Fig. 16. Pyridinic N is generally located at the edge or defects of graphene, pyrrolic N forms five-membered heterocyclic rings, and graphitic N represents N atoms that substitute carbon atoms within the graphene plane. Whereas contributions from different N functionalities towards ORR are still in debate, quaternary N is commonly believed to be unfavorable for the electrocatalytic process because of its tetrahedral sp^3 hybridization with a 3D structure that would interrupt the original planar structure and conjugation of the graphene $\pi-\pi$ electrons. In addition, it has been suggested that pyridinic N[139] and/or graphitic N[140] are actually responsible for the ORR performance. Interestingly, recent studies suggest equal contributions from both pyridinic and graphitic N for ORR.[141]

In a prior study based on DFT calculations,[141] it was found that edge-located carbons that were neighboring graphitic N atoms showed the lowest energy barrier for the first electron transfer of ORR. O_2 molecules first adsorbed on the active carbon atoms in an end-on manner (Fig. 17) and accepted protons as well as electrons. After releasing H_2O, the remaining adsorbed oxygen atom would cleave the C–N bond, forming a CHO group and a pyridinic N species. The pyridinic N then assisted the subsequent reduction of the remaining oxygen species, leading to eventual four-electron reduction. That is, both graphitic and pyridinic Ns were believed to be important for ORR.

Based on this mechanism (Fig. 17), high nitrogen contents are expected to be favored for enhanced ORR activity. However, too high a N content might be disadvantageous for ORR because of interruption of the $\pi-\pi$ electron conjugation and thus low electronic conductivity. Experimental work has indeed showed an unsatisfactory ORR performance with N-doped graphene that contains only pyridinic N but at a high concentration (16 at.%).[142] First-principle calculations also show that

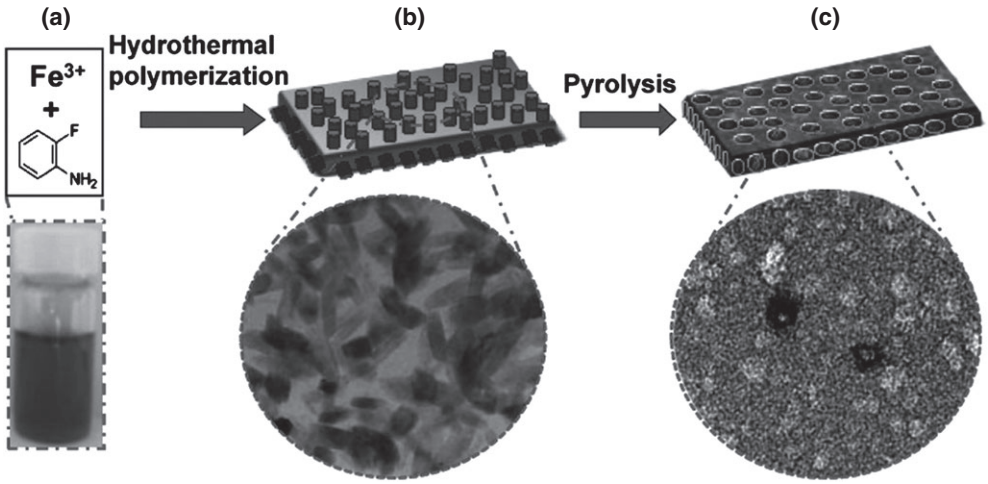

Figure 21. Schematic of the preparation process of Fe-N/C catalysts. Reproduced with permission from ref. 161.

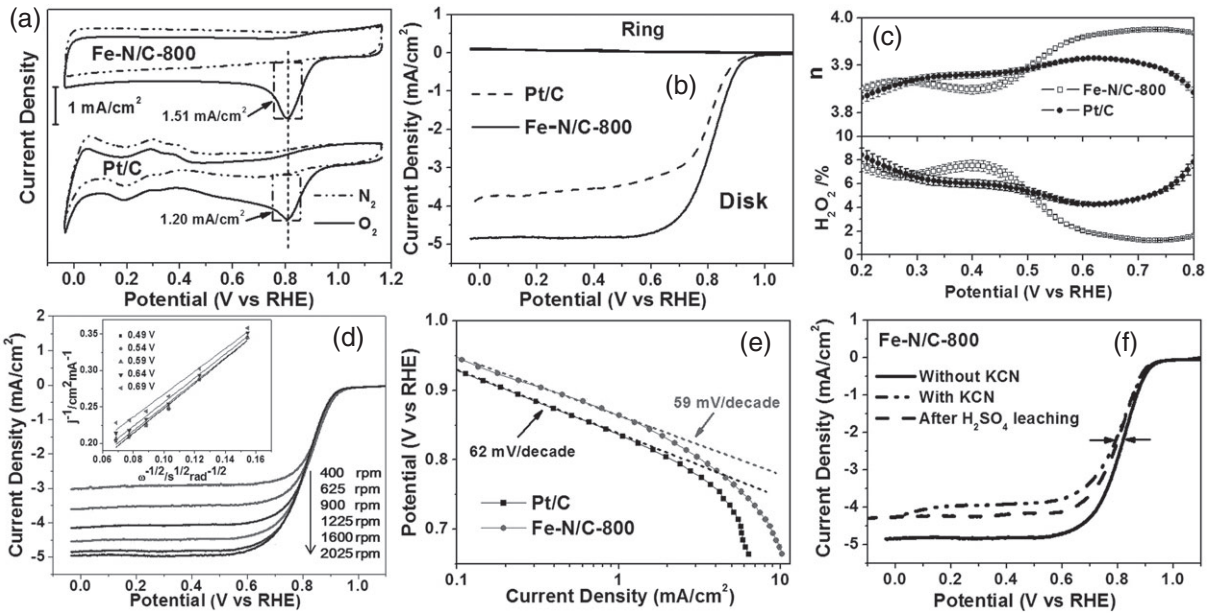

Figure 22. (a) Cyclic and (b) RRDE voltammograms, (c) plots of H_2O_2 yield and number of electron transfer of a GCE modified with Fe-N/C-800 and Pt/C catalysts at the rotation speed of 1600 rpm. (d) LSV curves for Fe-N/C-800 at the rotation rates of 400 to 2025 rpm; inset is the corresponding K-L plots at different potentials. (e) Corresponding Tafel plots of Fe-N/C-800 and Pt/C catalysts. (f) LSV curves of Fe-N/C-800 before (solid black) and after (dashed black) H_2SO_4 leaching treatments, and in 0.1 mol L^{-1} KOH aqueous solution with 10 mmol L^{-1} KCN (dashed grey). All measurements were conducted at a catalyst loading of 79.6 μg cm^{-2} in an O_2-saturated 0.1 mol L^{-1} KOH aqueous solution at a sweep rate of 10 mV s^{-1}. Reproduced with permission from ref. 161.

excessive B and N dopants can significantly increase the energy gap between the highest-occupied molecular orbital (HOMO) and the lowest-unoccupied molecular orbital (LUMO), and thus decrease the chemical reactivity of the doped carbons.[143] Theoretical studies have also shown that graphene with a higher nitrogen content will be more easily poisoned by adsorbed oxygen species due to stronger oxygen affinity.[144] These studies indicate that it is critical to optimize the nitrogen content for maximal ORR activity.

Dai *et al.*[145] claimed that the high electronegativity of N, compared with that of C, contributed to the high electrocatalytic activity of nitrogen-doped carbon nanotubes toward ORR. Based on this, it seems reasonable that carbon materials doped with heteroatoms such as F,[146] or I,[147] whose electronegativity is greater than that of C, will serve as even more efficient metal-free catalysts for ORR, and for P and B whose electronegativities are lower than that of C, the ORR activity should be minimal. However, experimentally, both P-[148] and B-doped[149] carbons show markedly enhanced ORR activity, an observation contradictory to the proposed mechanism. Furthermore, when carbon materials are doped by heteroatoms with electronegativity close to that of C, such as S[150] and Se,[120] one still observes apparent ORR activities. Therefore, it does not appear that the electroneutrality-breaking theory[149] is appropriate for explaining the unique ORR performance of heteroatom-doped carbon materials. Zhang *et al.*[151] suggested that the distribution of spin density might actually play a major role in the formation of catalytic active centers (Fig. 18), while contributions from atomic charge density might become significant if the spin density of an atom is small. Doping by foreign atoms can induce high spin density due to the introduction of unpaired single electrons, and DFT calculations have showed that

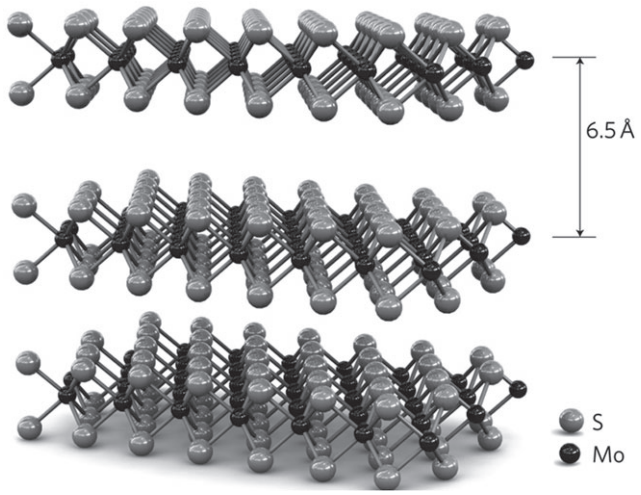

Figure 23. Depiction of MoS_2. Grey represents sulfur and black represents molybdenum. Reproduced with permission from ref. 170.

higher spin densities are favored for the adsorption of OOH, which is the initial step in ORR.[152] In the meantime, structural distortion induced by heteroatoms doping should be minimized; otherwise it will weaken the induced spin density. This may serve as a fundamental guideline in the selection of proper doping elements.

Compared with doping by single heteroatoms, recent studies have shown that codoping of carbon-based materials by nitrogen and other heteroatoms can further enhance the ORR performance due to the synergistic effects between the heteroatoms. For example, Wang *et al.*[143] developed a facile approach to prepare B,N co-doped graphene with tunable N-/B-doping levels through thermal annealing of GO in the presence of boric acid and ammonia. The resulting hybrids showed an ORR activity that was even better than that of commercial Pt/C. This was ascribed to the formation of a boron–carbon–nitride (BCN) structure; and first-principles calculations revealed that the energy bandgap, spin density and charge density were dependent on the doping level, where graphene with a moderate N- and B-doping level led to the best ORR electrocatalytic activity. However, in some other studies, the interpretation based on the formation of BCN was questioned, and instead, it was argued that the physical and chemical co-doping actually led to undesired side-products, including the above-mentioned BCN and hexagonal boron nitride (h-BN) which were chemically inert and behaved poorly in ORR. Zheng[153] developed an alternative two-step strategy to synthesize B,N-co-doped graphene by first annealing graphene with NH_3 at an intermediate temperature (e.g. 500 °C) and then introducing B by pyrolysis of the N-doped graphene with H_3BO_3 at a higher temperature (e.g. 900 °C). They claimed that this might prevent the formation of inactive side-products, and in fact, the resultant catalyst exhibited better ORR activity than was observed with B- or N-doped graphene via a one-step approach, within the context of onset potential, kinetic limiting current density, number of electron transfer and stability (Fig. 19).

In another study, Choi[154] synthesized P,N-dual doped carbon via pyrolysis of a mixture composed of dicyandiamide, phosphoric acid, cobalt chloride, and iron chloride at 900 °C under an Ar atmosphere. In comparison to N-doped carbon (Fig. 20(a)), the P dopants led to an uneven surface with increasing open edged sites (Fig. 20(b)–(e)), leading to an increase of the carbon surface area, which is beneficial for surface catalytic reactions. Furthermore, the additional P-doping resulted in more than four-fold enhancement in mass activity, with the 4e reduction pathway, as compared to that of N-doped carbon. In N,B-co-doped and N,P-co-doped carbon catalysts, one type of dopants (e.g. N) exhibited a higher electronegativity than carbon, whereas the other dopants (e.g. P, B) showed a lower electronegativity than carbon; therefore some believed that the synergistic coupling between the heteroatoms resulted in the formation of an unique electronic structure for ORR. It has also been argued that the additional doping of B or P led to enhanced asymmetry of the spin density or electron transfer on the basal plane of the graphene and thus decreased the HOMO-LUMO energy gap of graphene.[155] Yet this mechanism cannot be used to account for the results of N,S-co-doped carbon catalysts where the electronegativity of S is close to that of carbon. Experimentally, Liang *et al.*[156] synthesized N and S dual-doped mesoporous graphene (N,S-G) by heating a mixture of melamine/benzyl disulfide (BDS)/SiO_2 at a weight ratio of 5:5:1:5 at 900 °C in Ar to form N,S-G/SiO_2, where commercially available colloidal silica nanoparticles were employed to create large mesopores in the graphene catalysts. The resulting N,S-G hybrids exhibited an onset potential quite close to that of commercial Pt/C, which was much more positive than that of single doped or un-doped graphene, indicating that the dual-doping strategy was effective in developing highly-efficient metal-free catalysts for oxygen reduction reactions.

Research has also been carried out with ternary doping of carbon by, for instance, P, S and N,[157] where the motivation was to produce a large number of edge sites and increase the fraction of pyridinic-N sites in the carbon materials such that the ORR activity might be significantly enhanced.

In these studies, the ORR activity has been primarily ascribed to the doped carbons that serve as efficient ORR active sites. However, in some recent studies it has also been argued that the ORR activity may actually arise from trace amounts of metals in the carbon materials. In the experimental synthesis of GO by wet chemistry, chemical vapor deposition, or pyrolysis, metal compounds are typically involved. To address such an issue, Masa *et al.*[158] prepared N-modified carbon catalysts without the use of any metal precursors and then deliberately added trace metals into the carbon materials. They found that the pristine carbons did not show as good an ORR activity as the metal-modified ones. Researchers[159,160] also suggested that metal-related nanoparticles within the sp^2 carbon structures might significantly influence their electrocatalytic activities or even play a dominant role. Yet, in a recent study,[161] Niu *et al.* fabricated self-supported N-doped mesoporous carbons with FeO(OH) nanorods as thermally removable, rigid templates by combining hydrothermal synthesis and pyrolysis treatments at controlled temperatures (Fig. 21). The resulting mesoporous carbons exhibited a remarkable ORR activity with E_{onset} as positive as +0.98 V vs RHE, superior stability, and better tolerant ability against methanol poisoning than commercial Pt/C catalysts in alkaline media. They also found that substantial ORR activities were retained after cyanide poisoning or hot H_2SO_4 leaching (Fig. 22) which could block the Fe-based sites or remove metal (oxide) species. The results suggested that Fe-containing species were possibly involved in ORR but the contributions were likely small and graphitic N should be the predominant active components.

Note that whereas doped carbon materials show apparent catalytic activities towards ORR in alkaline media, their activities in acidic solutions are generally limited, compared with that of commercial Pt/C catalysts. Thus, doped carbons have been largely

used as a unique (but passive) support for nanoparticle catalysts in acidic media.[162–167] Indeed, it remains a challenge in developing effective carbon-based metal-free ORR catalysts in acid. This will largely depend on the understanding of the mechanistic origin of carbon-based ORR electrocatalysis.

SUMMARY AND PERSPECTIVES

In this article we have reviewed recent key progress in using graphene derivatives both as chemically robust substrates to support metal nanoparticles and as active metal-free catalysts for efficient electroreduction of oxygen. In these applications, graphene-based materials serve multiple purposes, for instance, to disperse metal nanoparticles and allow efficient charge transfer, and to impart electronic interactions so as to enhance the activity of the associated metal catalysts. Importantly, by deliberate doping of the molecular skeletons with heteroatoms, the carbons may even catalyze ORR without the incorporation of metal nanoparticles. In these studies, the structures of the graphene-based materials, in particular, the structural defects, are thought to play a critical role in the manipulation of the electronic interactions between the graphene substrates and the metal particles, as well as bonding interactions with oxygen and oxygen intermediates.

Despite substantial progress, much remains to be done. One critical aspect is to advance our understanding of the ORR mechanisms at these varied catalysts through novel theoretical and experimental design and evaluation. This will render it possible to differentiate the contributions/impacts of diverse structural parameters. Within such a fundamental framework, one may then achieve deliberate engineering of the structures and properties of the functional nanocomposites, such that the eventual electrocatalytic performance can be further enhanced and optimized.

Another critical area of research is to develop effective ORR catalysts based on other cost-effective, earth-abundant materials. For instance, other 2D layered materials such as molybdenum sulfide have also demonstrated catalytic activity toward oxygen reduction.[60,61,168,169] MoS_2 is a transition metal chalcogenide that displays a layered structure similar to graphene, with an extended network of alternating Mo and S atoms (Fig. 23).[170] Diverse synthetic techniques have been used, including hydrothermal methods,[171] scotch tape cleavage,[172] laser exfoliation,[173] solvent sonication,[174] and others.[175] The activity towards ORR has been recognized for MoS_2 nanoparticles and nanosheets,[168] and MoS_2/reduced graphene oxide (MoS_2/RGO) composites have been found to exhibit onset potential and ORR activity better than those of the individual constituents. Theoretical and experimental evidence suggests that the edges of the MoS_2 sheets are the catalytically active sites,[176–179] because of strong chemisorption of various molecules including O_2 at the edges.[180,181] However, the overall ORR activity of MoS_2 alone is generally rather low, compared with traditional platinoid metal catalysts. Thus, incorporation of metal nanoparticles is typically needed to enhance the ORR performance by taking advantage of the synergistic interactions between the two structural components and the formation of a unique interface.[60,182] Significant breakthroughs are needed to move forward in this area of research.

ACKNOWLEDGEMENTS

This work was supported in part by the National Science Foundation (CHE-1265635 and DMR-1409396).

REFERENCES

1 Cano-Castillo U, Hydrogen and fuel cells: potential elements in the energy transition scenario. *Rev Mex Fis* **59**:85–92 (2013).
2 Hamrock SJ, Herring AM and Zawodzinski TA, Fuel cell chemistry and operation. *J Power Sources* **172**:1 (2007).
3 Patel A, Artyushkova K, Atanassov P, Colbow V, Dutta M, Harvey D and Wessel S, Investigating the effects of proton exchange membrane fuel cell conditions on carbon supported platinum electrocatalyst composition and performance. *J Vac Sci Technol A* **30**:04D107 (2012).
4 Borup R, Meyers J, Pivovar B, Kim YS, Mukundan R, Garland N *et al.*, Scientific aspects of polymer electrolyte fuel cell durability and degradation. *Chem Rev* **107**:3904–3951 (2007).
5 Stephens IEL, Bondarenko AS, Grønbjerg U, Rossmeisl J and Chorkendorff I, Understanding the electrocatalysis of oxygen reduction on platinum and its alloys. *Energy Environ Sci* **5**:6744 (2012).
6 Norskov JK, Rossmeisl J, Logadottir A, Lindqvist L, Kitchin JR, Bligaard T and Jonsson H, Origin of the overpotential for oxygen reduction at a fuel-cell cathode. *J Phys Chem B* **108**:17886–17892 (2004).
7 Ramaswamy N and Mukerjee S, Fundamental mechanistic understanding of electrocatalysis of oxygen reduction on Pt and non-Pt surfaces: acid versus alkaline media. *Adv Phys Chem* 2012:1–17 (**2012**).
8 Lim D-H and Wilcox J, Mechanisms of the oxygen reduction reaction on defective graphene-supported Pt nanoparticles from first-principles. *J Phys Chem C* **116**:3653–3660 (2012).
9 Lima FHB, Zhang J, Shao MH, Sasaki K, Vukmirovic MB, Ticianelli EA and Adzic RR, Catalytic activity-d-band center correlation for the O2 reduction reaction on platinum in alkaline solutions. *J Phys Chem C* **111**:404–410 (2007).
10 Kitchin JR, Norskov JK, Barteau MA and Chen JG, Modification of the surface electronic and chemical properties of Pt(111) by subsurface 3d transition metals. *J Chem Phys* **120**:10240–10246 (2004).
11 Stephens IE, Bondarenko AS, Perez-Alonso FJ, Calle-Vallejo F, Bech L, Johansson TP, Jepsen AK, Frydendal R, Knudsen BP, Rossmeisl J and Chorkendorff I, Tuning the activity of Pt(111) for oxygen electroreduction by subsurface alloying. *J Am Chem Soc* **133**:5485–5491 (2011).
12 Greeley J, Stephens IEL, Bondarenko AS, Johansson TP, Hansen HA, Jaramillo TF, Rossmeisl J, Chorkendorff I and Norskov JK, Alloys of platinum and early transition metals as oxygen reduction electrocatalysts. *Nat Chem* **1**:552–556 (2009).
13 Greeley J and Norskov JK, Combinatorial density functional theory-based screening of surface alloys for the oxygen reduction reaction. *J Phys Chem C* **113**:4932–4939 (2009).
14 Hammer B and Norskov JK, Electronic factors determining the reactivity of metal surfaces. *Surf Sci* **343**:211–220 (1995).
15 Hennig D, Ganduglia Pirovano MV and Scheffler M, Adlayer core-level shifts of admetal monolayers on transition-metal substrates and their relation to the surface chemical reactivity. *Phys Rev B* **53**:10344–10347 (1996).
16 Bzowski A, Sham TK, Watson RE and Weinert M, Electronic-structure of Au and Ag overlayers on Ru(001) - the behavior of the noble-metal D-bands. *Phys Rev B* **51**:9979–9984 (1995).
17 Weinert M and Watson RE, Core-level shifts in bulk alloys and surface adlayers. *Phys Rev B* **51**:17168–17180 (1995).
18 Toyoda E, Jinnouchi R, Hatanaka T, Morimoto Y, Mitsuhara K, Visikovskiy A and Kido Y, The d-band structure of Pt nanoclusters correlated with the catalytic activity for an oxygen reduction reaction. *J Phys Chem C* **115**:21236–21240 (2011).
19 Carpenter MK, Moylan TE, Kukreja RS, Atwan MH and Tessema MM, Solvothermal synthesis of platinum alloy nanoparticles for oxygen reduction electrocatalysis. *J Am Chem Soc* **134**:8535–8542 (2012).
20 Seo A, Lee J, Han K and Kim H, Performance and stability of Pt-based ternary alloy catalysts for PEMFC. *Electrochim Acta* **52**:1603–1611 (2006).
21 Stamenkovic VR, Fowler B, Mun BS, Wang G, Ross PN, Lucas CA and Markovic NM, Improved oxygen reduction activity on Pt3Ni(111) via increased surface site availability. *Science* **315**:493–497 (2007).
22 Luo J, Njoki PN, Lin Y, Wang LY and Zhong CJ, Activity-composition correlation of AuPt alloy nanoparticle catalysts in electrocatalytic reduction of oxygen. *Electrochem Commun* **8**:581–587 (2006).
23 Paalanen P, Weckhuysen BM and Sankar M, Progress in controlling the size, composition and nanostructure of supported gold–palladium nanoparticles for catalytic applications. *Catal Sci Technol* **3**:2869 (2013).

24 Liu Y, Zhang L, Willis BG and Mustain WE, Importance of particle size and distribution in achieving high-activity, high-stability oxygen reduction catalysts. *ACS Catal* **5**:1560–1567 (2015).
25 Zhou WJ, Li M, Ding OL, Chan SH, Zhang L and Xue YH, Pd particle size effects on oxygen electrochemical reduction. *Int J Hydrogen Energy* **39**:6433–6442 (2014).
26 Shao MH, Peles A and Shoemaker K, Electrocatalysis on platinum nanoparticles: particle size effect on oxygen reduction reaction activity. *Nano Lett* **11**:3714–3719 (2011).
27 Kim JW, Lim B, Jang HS, Hwang SJ, Yoo SJ, Ha JS, Cho EA, Lim TH, Nam SW and Kim SK, Size-controlled synthesis of Pt nanoparticles and their electrochemical activities toward oxygen reduction. *Int J Hydrogen Energy* **36**:706–712 (2011).
28 Wang JX, Inada H, Wu LJ, Zhu YM, Choi YM, Liu P *et al.*, Oxygen reduction on well-defined core-shell nanocatalysts: particle size, facet, and Pt shell thickness effects. *J Am Chem Soc* **131**:17298–17302 (2009).
29 Wu J, Zhang J, Peng ZM, Yang SC, Wagner FT and Yang H, Truncated octahedral Pt3Ni oxygen reduction reaction electrocatalysts. *J Am Chem Soc* **132**:4984–4985 (2010).
30 Lee C-L, Chiou H-P, Syu C-M and Wu C-C, Silver triangular nanoplates as electrocatalyst for oxygen reduction reaction. *Electrochem Commun* **12**:1609–1613 (2010).
31 Shao M, Odell J, Humbert M, Yu T and Xia Y, Electrocatalysis on shape-controlled palladium nanocrystals: oxygen reduction reaction and formic acid oxidation. *J Phys Chem C* **117**:4172–4180 (2013).
32 He G, Song Y, Phebus B, Liu K, Deming CP, Hu P and Chen S, Electrocatalytic activity of organically functionalized silver nanoparticles in oxygen reduction. *Sci Adv Mater* **5**:1727–1736 (2013).
33 Liu K, Kang X, Zhou Z-Y, Song Y, Lee LJ, Tian D and Chen S, Platinum nanoparticles functionalized with acetylene derivatives: electronic conductivity and electrocatalytic activity in oxygen reduction. *J Electroanal Chem* **688**:143–150 (2013).
34 Zhou ZY, Kang X, Song Y and Chen S, Enhancement of the electrocatalytic activity of Pt nanoparticles in oxygen reduction by chlorophenyl functionalization. *Chem Commun (Camb)* **48**:3391–3393 (2012).
35 Zhou Z-Y, Kang X, Song Y and Chen S, Ligand-mediated electrocatalytic activity of Pt nanoparticles for oxygen reduction reactions. *J Phys Chem C* **116**:10592–10598 (2012).
36 Pietron JJ, Garsany Y, Baturina O, Swider-Lyons KE, Stroud RM, Ramaker DE and Schull TL, Electrochemical observation of ligand effects on oxygen reduction at ligand-stabilized Pt nanoparticle electrocatalysts. *Electrochem Solid-State Lett* **11**:B161 (2008).
37 Kongkanand A, Kuwabata S, Girishkumar G and Kamat P, Single-wall carbon nanotubes supported platinum nanoparticles with improved electrocatalytic activity for oxygen reduction reaction. *Langmuir* **22**:2392–2396 (2006).
38 Li WZ, Liang CH, Zhou WJ, Qiu JS, Zhou ZH, Sun GQ and Xin Q, Preparation and characterization of multiwalled carbon nanotube-supported platinum for cathode catalysts of direct methanol fuel cells. *J Phys Chem B* **107**:6292–6299 (2003).
39 Joo SH, Kwon K, You DJ, Pak C, Chang H and Kim JM, Preparation of high loading Pt nanoparticles on ordered mesoporous carbon with a controlled Pt size and its effects on oxygen reduction and methanol oxidation reactions. *Electrochim Acta* **54**:5746–5753 (2009).
40 Ding J, Chan KY, Ren JW and Xiao FS, Platinum and platinum-ruthenium nanoparticles supported on ordered mesoporous carbon and their electrocatalytic performance for fuel cell reactions. *Electrochim Acta* **50**:3131–3141 (2005).
41 Wen ZH, Liu J and Li JH, Core/shell Pt/C nanoparticles embedded in mesoporous carbon as a methanol-tolerant cathode catalyst in direct methanol fuel cells. *Adv Mater* **20**:743–747 (2008).
42 Hsin YL, Hwang KC and Yeh CT, Poly(vinylpyrrolidone)-modified graphite carbon nanofibers as promising supports for PtRu catalysts in direct methanol fuel cells. *J Am Chem Soc* **129**:9999–10010 (2007).
43 Jia JC, Wang H, Ji S, Yang HJ, Li XS and Wang RF, SnO2-embedded worm-like carbon nanofibers supported Pt nanoparticles for oxygen reduction reaction. *Electrochim Acta* **141**:13–19 (2014).
44 He GQ, Song Y, Liu K, Walter A, Chen S and Chen SW, Oxygen reduction catalyzed by platinum nanoparticles supported on graphene quantum dots. *ACS Catal* **3**:831–838 (2013).
45 Song Y and Chen SW, Graphene quantum-dot-supported platinum nanoparticles: defect-mediated electrocatalytic activity in oxygen reduction. *ACS Appl Mater Interfaces* **6**:14050–14060 (2014).
46 Liang YY, Li YG, Wang HL, Zhou JG, Wang J, Regier T and Dai HJ, Co3O4 nanocrystals on graphene as a synergistic catalyst for oxygen reduction reaction. *Nat Mater* **10**:780–786 (2011).
47 Wu Z-S, Yang S, Sun Y, Parvez K, Feng X and Müllen K, 3D Nitrogen-doped graphene aerogel-supported Fe3O4 nanoparticles as efficient electrocatalysts for the oxygen reduction reaction. *J Am Chem Soc* **134**:9082–9085 (2012).
48 Zhou XJ, Qiao JL, Yang L and Zhang JJ, A review of graphene-based nanostructural materials for both catalyst supports and metal-free catalysts in PEM fuel cell oxygen reduction reactions. *Adv Energy Mater* **4**:201301523 (2014).
49 Sharma S and Pollet BG, Support materials for PEMFC and DMFC electrocatalysts - a review. *J Power Sources* **208**:96–119 (2012).
50 Price SWT, Thompson SJ, Li X, Gorman SF, Pletcher D, Russell AE, Walsh FC and Wills RGA, The fabrication of a bifunctional oxygen electrode without carbon components for alkaline secondary batteries. *J Power Sources* **259**:43–49 (2014).
51 Low CTJ, Walsh FC, Chakrabarti MH, Hashim MA and Hussain MA, Electrochemical approaches to the production of graphene flakes and their potential applications. *Carbon* **54**:1–21 (2013).
52 Geim AK and Novoselov KS, The rise of graphene. *Nat Mater* **6**:183–191 (2007).
53 Geng DS, Chen Y, Chen YG, Li YL, Li RY, Sun XL, Ye SY and Knights S, High oxygen-reduction activity and durability of nitrogen-doped graphene. *Energy Environ Sci* **4**:760–764 (2011).
54 Sheng ZH, Gao HL, Bao WJ, Wang FB and Xia XH, Synthesis of boron doped graphene for oxygen reduction reaction in fuel cells. *J Mater Chem* **22**:390–395 (2012).
55 Jin Z, Yao J, Kittrell C and Tour JM, Large-scale growth and characterizations of nitrogen-doped monolayer graphene sheets. *ACS Nano* **5**:4112–4117 (2011).
56 Qu LT, Liu Y, Baek JB and Dai LM, Nitrogen-doped graphene as efficient metal-free electrocatalyst for oxygen reduction in fuel cells. *ACS Nano* **4**:1321–1326 (2010).
57 Yu DS, Zhang Q and Dai LM, Highly efficient metal-free growth of nitrogen-doped single-walled carbon nanotubes on plasma-etched substrates for oxygen reduction. *J Am Chem Soc* **132**:15127–15129 (2010).
58 Qu D, Zheng M, Du P, Zhou Y, Zhang L, Li D, Tan H, Zhao Z, Xie Z and Sun Z, Highly luminescent S, N co-doped graphene quantum dots with broad visible absorption bands for visible light photocatalysts. *Nanoscale* **5**:12272–12277 (2013).
59 Deng D, Pan X, Yu L, Cui Y, Jiang Y, Qi J, Li W-X, Fu Q, Ma X, Xue Q, Sun G and Bao X, Toward N-doped graphene via solvothermal synthesis. *Chem Mater* **23**:1188–1193 (2011).
60 Wang TY, Zhuo JQ, Chen Y, Du KZ, Papakonstantinou P, Zhu ZW, Shao YH and Li MX, Synergistic catalytic effect of MoS2 nanoparticles supported on gold nanoparticle films for a highly efficient oxygen reduction reaction. *Chemcatchem* **6**:1877–1881 (2014).
61 Rao CN, Gopalakrishnan K and Maitra U, Comparative study of potential applications of graphene, MoS2, and other two-dimensional materials in energy devices, sensors, and related areas. *ACS Appl Mater Interfaces* **7**:7809–7832 (2015).
62 Chianelli RR, Siadati MH, De la Rosa MP, Berhault G, Wilcoxon JP, Bearden R and Abrams BL, Catalytic properties of single layers of transition metal sulfide catalytic materials. *Catal Rev* **48**:1–41 (2006).
63 Hinnemann B, Moses PG, Bonde J, Jorgensen KP, Nielsen JH, Horch S, Chorkendorff I and Norskov JK, Biornimetic hydrogen evolution: MoS2 nanoparticles as catalyst for hydrogen evolution. *J Am Chem Soc* **127**:5308–5309 (2005).
64 Kauffman DR and Star A, Graphene versus carbon nanotubes for chemical sensor and fuel cell applications. *Analyst* **135**:2790–2797 (2010).
65 Antolini E, Graphene as a new carbon support for low-temperature fuel cell catalysts. *Appl Catal B: Environ* **123–124**:52–68 (2012).
66 Kou R, Shao YY, Wang DH, Engelhard MH, Kwak JH, Wang J, Viswanathan VV, Wang CM, Lin YH, Wang Y, Aksay IA and Liu J, Enhanced activity and stability of Pt catalysts on functionalized graphene sheets for electrocatalytic oxygen reduction. *Electrochem Commun* **11**:954–957 (2009).

67 Shao YY, Zhang S, Wang CM, Nie ZM, Liu J, Wang Y and Lin YH, Highly durable graphene nanoplatelets supported Pt nanocatalysts for oxygen reduction. *J Power Sources* **195**:4600–4605 (2010).
68 Song WY, Chen ZX, Yang C, Yang ZP, Tai JP, Nan YL *et al.*, Carbon-coated, methanol-tolerant platinum/graphene catalysts for oxygen reduction reaction with excellent long-term performance. *J Mater Chem A* **3**:1049–1057 (2015).
69 Rao CV, Reddy ALM, Ishikawa Y and Ajayan PM, Synthesis and electrocatalytic oxygen reduction activity of graphene-supported Pt3Co and Pt3Cr alloy nanoparticles. *Carbon* **49**:931–936 (2011).
70 Zhang K, Yue QL, Chen GF, Zhai YL, Wang L, Wang HS, Zhao JS, Liu JF, Jia JB and Li HB, Effects of acid treatment of Pt-Ni alloy nanoparticles@Graphene on the kinetics of the oxygen reduction reaction in acidic and alkaline solutions. *J Phys Chem C* **115**:379–389 (2011).
71 Tiwari JN, Nath K, Kumar S, Tiwari RN, Kemp KC, Le NH, Youn DH, Lee JS and Kim KS, Stable platinum nanoclusters on genomic DNA-graphene oxide with a high oxygen reduction reaction activity. *Nat Commun* **4**:2221 (2013).
72 Hoque MA, Hassan FM, Higgins D, Choi JY, Pritzker M, Knights S, Ye SY and Chen ZW, Multigrain platinum nanowires consisting of oriented nanoparticles anchored on sulfur-doped graphene as a highly active and durable oxygen reduction electrocatalyst. *Adv Mater* **27**:1229–1234 (2015).
73 Navaee A, Salimi A, Soltanian S and Servati P, Facile one-pot synthesis of platinum nanoparticles decorated nitrogen-graphene with high electrocatalytic performance for oxygen reduction and anodic fuels oxidation. *J Power Sources* **277**:268–276 (2015).
74 Higgins D, Hoque MA, Seo MH, Wang RY, Hassan F, Choi JY, Pritzker M, Yu AP, Zhang JJ and Chen ZW, Development and simulation of sulfur-doped graphene supported platinum with exemplary stability and activity towards oxygen reduction. *Adv Funct Mater* **24**:4325–4336 (2014).
75 Li YJ, Li YJ, Zhu EB, McLouth T, Chiu CY, Huang XQ and Huang Y, Stabilization of high-performance oxygen reduction reaction Pt electrocatalyst supported on reduced graphene oxide/carbon black composite. *J Am Chem Soc* **134**:12326–12329 (2012).
76 Arenz M, Stamenkovic V, Schmidt TJ, Wandelt K, Ross PN and Markovic NM, The electro-oxidation of formic acid on Pt-Pd single crystal bimetallic surfaces. *Phys Chem Chem Phys* **5**:4242–4251 (2003).
77 Chen XM, Wu GH, Chen JM, Chen X, Xie ZX and Wang XR, Synthesis of 'clean' and well-dispersive Pd nanoparticles with excellent electrocatalytic property on graphene oxide. *J Am Chem Soc* **133**:3693–3695 (2011).
78 Yang J, Tian CG, Wang L and Fu HG, An effective strategy for small-sized and highly-dispersed palladium nanoparticles supported on graphene with excellent performance for formic acid oxidation. *J Mater Chem* **21**:3384–3390 (2011).
79 Gotoh K, Kawabata K, Fujii E, Morishige K, Kinumoto T, Miyazaki Y and Ishida H, The use of graphite oxide to produce mesoporous carbon supporting Pt, Ru, or Pd nanoparticles. *Carbon* **47**:2120–2124 (2009).
80 Xu C, Wang X and Zhu JW, Graphene-metal particle nanocomposites. *J Phys Chem C* **112**:19841–19845 (2008).
81 Liu X, Li L, Meng C and Han Y, Palladium nanoparticles/defective graphene composites as oxygen reduction electrocatalysts: a first-principles study. *J Phys Chem C* **116**:2710–2719 (2012).
82 Seo MH, Choi SM, Kim HJ and Kim WB, The graphene-supported Pd and Pt catalysts for highly active oxygen reduction reaction in an alkaline condition. *Electrochem Commun* **13**:182–185 (2011).
83 Truong-Phuoc L, Pham-Huu C, Da Costa V and Janowska I, Few-layered graphene-supported palladium as a highly efficient catalyst in oxygen reduction reaction. *Chem Commun* **50**:14433–14435 (2014).
84 Arenz M, Schmidt TJ, Wandelt K, Ross PN and Markovic NM, The oxygen reduction reaction on thin palladium films supported on a Pt(111) electrode. *J Phys Chem B* **107**:9813–9819 (2003).
85 Wells PP, Crabb EM, King CR, Wiltshire R, Billsborrow B, Thompsett D and Russell AE, Preparation, structure, and stability of Pt and Pd monolayer modified Pd and Pt electrocatalysts. *Phys Chem Chem Phys* **11**:5773–5781 (2009).
86 Haruta M, Yamada N, Kobayashi T and Iijima S, Gold catalysts prepared by coprecipitation for low-temperature oxidation of hydrogen and of carbon-monoxide. *J Catal* **115**:301–309 (1989).
87 Chen W and Chen SW, Oxygen electroreduction catalyzed by gold nanoclusters: strong core size effects. *Angew Chem Int Ed* **48**:4386–4389 (2009).
88 Yagi I, Ishida T and Uosaki K, Electrocatalytic reduction of oxygen to water at Au nanoclusters vacuum-evaporated on boron-doped diamond in acidic solution. *Electrochem Commun* **6**:773–779 (2004).
89 Hernandez J, Solla-Gullon J, Herrero E, Aldaz A and Feliu JM, Electrochemistry of shape-controlled catalysts: oxygen reduction reaction on cubic gold nanoparticles. *J Phys Chem C* **111**:14078–14083 (2007).
90 Li XR, Li XL, Xu MC, Xu JJ and Chen HY, Gold nanodendrities on graphene oxide nanosheets for oxygen reduction reaction. *J Mater Chem A* **2**:1697–1703 (2014).
91 Xu SJ, Yong L and Wu PY, One-pot, green, rapid synthesis of flower-like gold nanoparticles/reduced graphene oxide composite with regenerated silk fibroin as efficient oxygen reduction electrocatalysts. *ACS Appl Mater Interfaces* **5**:654–662 (2013).
92 Xu SJ and Wu PY, Facile and green synthesis of a surfactant-free Au clusters/reduced graphene oxide composite as an efficient electrocatalyst for the oxygen reduction reaction. *J Mater Chem A* **2**:13682–13690 (2014).
93 Yin HJ, Tang HJ, Wang D, Gao Y and Tang ZY, Facile synthesis of surfactant-free Au cluster/graphene hybrids for high-performance oxygen reduction reaction. *ACS Nano* **6**:8288–8297 (2012).
94 Govindhan M and Chen AC, Simultaneous synthesis of gold nanoparticle/graphene nanocomposite for enhanced oxygen reduction reaction. *J Power Sources* **274**:928–936 (2015).
95 Wang FB, Wang J, Shao L, Zhao Y and Xia XH, Hybrids of gold nanoparticles highly dispersed on graphene for the oxygen reduction reaction. *Electrochem Commun* **38**:82–85 (2014).
96 Guo JS, Hsu A, Chu D and Chen RR, Improving oxygen reduction reaction activities on carbon-supported Ag nanoparticles in alkaline solutions. *J Phys Chem C* **114**:4324–330 (2010).
97 Chatenet M, Genies-Bultel L, Aurousseau M, Durand R and Andolfatto F, Oxygen reduction on silver catalysts in solutions containing various concentrations of sodium hydroxide - comparison with platinum. *J Appl Electrochem* **32**:1131–1140 (2002).
98 Lim EJ, Choi SM, Seo MH, Kim Y, Lee S and Kim WB, Highly dispersed Ag nanoparticles on nanosheets of reduced graphene oxide for oxygen reduction reaction in alkaline media. *Electrochem Commun* **28**:100–103 (2013).
99 Lee K, Ahmed MS and Jeon S, Various carbon chain containing linkages grafted graphene with silver nanoparticles electrocatalysts for oxygen reduction reaction. *J Electrochem Soc* **162**:F1–F8 (2015).
100 Zhou RF, Zheng Y, Hulicova-Jurcakova D and Qiao SZ, Enhanced electrochemical catalytic activity by copper oxide grown on nitrogen-doped reduced graphene oxide. *J Mater Chem A* **1**:13179–13185 (2013).
101 Lv JJ, Li SS, Wang AJ, Mei LP, Feng JJ, Chen JR and Chen ZJ, One-pot synthesis of monodisperse palladium-copper nanocrystals supported on reduced graphene oxide nanosheets with improved catalytic activity and methanol tolerance for oxygen reduction reaction. *J Power Sources* **269**:104–110 (2014).
102 Zheng YL, Zhao SL, Liu SL, Yin HH, Chen YY, Bao JC, Han M and Dai ZH, Component-controlled synthesis and assembly of Cu-Pd nanocrystals on graphene for oxygen reduction reaction. *ACS Appl Mater Interfaces* **7**:5347–5357 (2015).
103 Liu X, Meng CG and Han Y, Defective graphene supported MPd12 (M = Fe, Co, Ni, Cu, Zn, Pd) nanoparticles as potential oxygen reduction electrocatalysts: a first-principles study. *J Phys Chem C* **117**:1350–1357 (2013).
104 Guo SJ and Sun SH, FePt nanoparticles assembled on graphene as enhanced catalyst for oxygen reduction reaction. *J Am Chem Soc* **134**:2492–2495 (2012).
105 Khan M, Bin Yousaf A, Chen MM, Wei CS, Wu XB, Huang ND, Qi ZM and Li L, Mixed-phase Pd-Pt bimetallic alloy on graphene oxide with high activity for electrocatalytic applications. *J Power Sources* **282**:520–528 (2015).
106 Guo SJ, Zhang S, Wu LH and Sun SH, Co/CoO nanoparticles assembled on graphene for electrochemical reduction of oxygen. *Angew Chem Int Ed* **51**:11770–11773 (2012).
107 Wu ZX, Lv YY, Xia YY, Webley PA and Zhao DY, Ordered mesoporous platinum@Graphitic carbon embedded nanophase as a highly active, stable, and methanol-tolerant oxygen reduction electrocatalyst. *J Am Chem Soc* **134**:2236–2245 (2012).
108 Li L and Xing YC, Electrochemical durability of carbon nanotubes in noncatalyzed and catalyzed oxidations. *J Electrochem Soc* **153**:A1823–A1828 (2006).

109 Wang JJ, Yin GP, Shao YY, Wang ZB and Gao YZ, Investigation of further improvement of platinum catalyst durability with highly graphitized carbon nanotubes support. *J Phys Chem C* **112**:5784–5789 (2008).

110 He DP, Cheng K, Peng T, Sun XL, Pan M and Mu SC, Bifunctional effect of reduced graphene oxides to support active metal nanoparticles for oxygen reduction reaction and stability. *J Mater Chem* **22**:21298–21304 (2012).

111 Chen SW, Templeton AC and Murray RW, Monolayer-protected cluster growth dynamics. *Langmuir* **16**:3543–3548 (2000).

112 Ma JW, Habrioux A, Luo Y, Ramos-Sanchez G, Calvillo L, Granozzi G *et al.*, Electronic interaction between platinum nanoparticles and nitrogen-doped reduced graphene oxide: effect on the oxygen reduction reaction. *J Mater Chem A* **3**:11891–11904 (2015).

113 Gao W, Mueller JE, Anton J, Jiang Q and Jacob T, Nickel cluster growth on defect sites of graphene: a computational study. *Angew Chem Int Ed* **52**:14237–14241 (2013).

114 Li XH and Antonietti M, Metal nanoparticles at mesoporous N-doped carbons and carbon nitrides: functional Mott-Schottky heterojunctions for catalysis. *Chem Soc Rev* **42**:6593–6604 (2013).

115 Lv LB, Ye TN, Gong LH, Wang KX, Su J, Li XH and Chen JS, Anchoring cobalt nanocrystals through the plane of graphene: highly integrated electrocatalyst for oxygen reduction reaction. *Chem Mater* **27**:544–549 (2015).

116 Hou Y, Wen ZH, Cui SM, Ci SQ, Mao S and Chen JH, An advanced nitrogen-doped graphene/cobalt-embedded porous carbon polyhedron hybrid for efficient catalysis of oxygen reduction and water splitting. *Adv Funct Mater* **25**:872–882 (2015).

117 Jiang S, Zhu CZ and Dong SJ, Cobalt and nitrogen-cofunctionalized graphene as a durable non-precious metal catalyst with enhanced ORR activity. *J Mater Chem A* **1**:3593–3599 (2013).

118 Lee DU, Kim BJ and Chen ZW, One-pot synthesis of a mesoporous NiCo2O4 nanoplatelet and graphene hybrid and its oxygen reduction and evolution activities as an efficient bi-functional electrocatalyst. *J Mater Chem A* **1**:4754–4762 (2013).

119 An L, Huang WF, Zhang NL, Chen X and Xia DG, A novel CoN electrocatalyst with high activity and stability toward oxygen reduction reaction. *J Mater Chem A* **2**:62–65 (2014).

120 Jin ZP, Nie HG, Yang Z, Zhang J, Liu Z, Xu XJ and Huang SM, Metal-free selenium doped carbon nanotube/graphene networks as a synergistically improved cathode catalyst for oxygen reduction reaction. *Nanoscale* **4**:6455–6460 (2012).

121 Wei DC, Liu YQ, Wang Y, Zhang HL, Huang LP and Yu G, Synthesis of N-doped graphene by chemical vapor deposition and its electrical properties. *Nano Lett* **9**:1752–1758 (2009).

122 Cattelan M, Agnoli S, Favaro M, Garoli D, Romanato F, Meneghetti M, Barinov A, Dudin P and Granozzi G, Microscopic view on a chemical vapor deposition route to boron-doped graphene nanostructures. *Chem Mater* **25**:1490–1495 (2013).

123 Wu TR, Shen HL, Sun L, Cheng B, Liu B and Shen JC, Nitrogen and boron doped monolayer graphene by chemical vapor deposition using polystyrene, urea and boric acid. *New J Chem* **36**:1385–1391 (2012).

124 Gao H, Liu Z, Song L, Guo WH, Gao W, Ci LJ, Rao A, Quan WJ, Vajtai R and Ajayan PM, Synthesis of S-doped graphene by liquid precursor. *Nanotechnology* **23**:275605 (2012).

125 Liu X, Li L, Zhou W, Zhou Y, Niu W and Chen S, High-performance electrocatalysts for oxygen reduction based on nitrogen-doped porous carbon from hydrothermal treatment of glucose and dicyandiamide. *ChemElectroChem* **2**:803–810 (2015).

126 Zheng Y, Jiao Y, Chen J, Liu J, Liang J, Du A, Zhang WM, Zhu ZH, Smith SC, Jaroniec M, Lu GQ and Qiao SZ, Nanoporous graphitic-C3N4@Carbon metal-free electrocatalysts for highly efficient oxygen reduction. *J Am Chem Soc* **133**:20116–20119 (2011).

127 Nallathambi V, Lee JW, Kumaraguru SP, Wu G and Popov BN, Development of high performance carbon composite catalyst for oxygen reduction reaction in PEM Proton Exchange Membrane fuel cells. *J Power Sources* **183**:34–42 (2008).

128 Wu G, Dai CS, Wang DL, Li DY and Li N, Nitrogen-doped magnetic onion-like carbon as support for Pt particles in a hybrid cathode catalyst for fuel cells. *J Mater Chem* **20**:3059–3068 (2010).

129 Lee JS, Park GS, Kim ST, Liu ML and Cho J, A highly efficient electrocatalyst for the oxygen reduction reaction: N-doped ketjenblack incorporated into Fe/Fe3C-functionalized melamine foam. *Angew Chem Int Ed* **52**:1026–1030 (2013).

130 Zhao Y, Watanabe K and Hashimoto K, Self-supporting oxygen reduction electrocatalysts made from a nitrogen-rich network polymer. *J Am Chem Soc* **134**:19528–19531 (2012).

131 Zhong M, Kim EK, McGann JP, Chun SE, Whitacre JF, Jaroniec M, Matyjaszewski K and Kowalewski T, Electrochemically active nitrogen-enriched nanocarbons with well-defined morphology synthesized by pyrolysis of self-assembled block copolymer. *J Am Chem Soc* **134**:14846–14857 (2012).

132 Zhou K, Zhou WJ, Liu XJ, Wang Y, Wan JQ and Chen SW, Nitrogen self-doped porous carbon from surplus sludge as metal-free electrocatalysts for oxygen reduction reactions. *ACS Appl Mater Interfaces* **6**:14911–14918 (2014).

133 Liu XJ, Zhou YC, Zhou WJ, Li LG, Huang SB and Chen SW, Biomass-derived nitrogen self-doped porous carbon as effective metal-free catalysts for oxygen reduction reaction. *Nanoscale* **7**:6136–6142 (2015).

134 Wang XR, Li XL, Zhang L, Yoon Y, Weber PK, Wang HL, Guo J and Dai HJ, N-doping of graphene through electrothermal reactions with ammonia. *Science* **324**:768–771 (2009).

135 Sheng ZH, Shao L, Chen JJ, Bao WJ, Wang FB and Xia XH, Catalyst-free synthesis of nitrogen-doped graphene via thermal annealing graphite oxide with melamine and its excellent electrocatalysis. *ACS Nano* **5**:4350–4358 (2011).

136 Lu ZJ, Bao SJ, Gou YT, Cai CJ, Ji CC, Xu MW, Song J and Wang RY, Nitrogen-doped reduced-graphene oxide as an efficient metal-free electrocatalyst for oxygen reduction in fuel cells. *RSC Adv* **3**:3990–3995 (2013).

137 Wu JJ, Zhang D, Wang Y and Hou BR, Electrocatalytic activity of nitrogen-doped graphene synthesized via a one-pot hydrothermal process towards oxygen reduction reaction. *J Power Sources* **227**:185–190 (2013).

138 Zhang YJ, Fugane K, Mori T, Niu L and Ye JH, Wet chemical synthesis of nitrogen-doped graphene towards oxygen reduction electrocatalysts without high-temperateure pyrolysis. *J Mater Chem* **22**:6575–6580 (2012).

139 Subramanian NP, Li XG, Nallathambi V, Kumaraguru SP, Colon-Mercado H, Wu G, Lee JW and Popov BN, Nitrogen-modified carbon-based catalysts for oxygen reduction reaction in polymer electrolyte membrane fuel cells. *J Power Sources* **188**:38–44 (2009).

140 Niwa H, Horiba K, Harada Y, Oshima M, Ikeda T, Terakura K, Ozaki J and Miyata S, X-ray absorption analysis of nitrogen contribution to oxygen reduction reaction in carbon alloy cathode catalysts for polymer electrolyte fuel cells. *J Power Sources* **187**:93–97 (2009).

141 Kim H, Lee K, Woo SI and Jung Y, On the mechanism of enhanced oxygen reduction reaction in nitrogen-doped graphene nanoribbons. *Phys Chem Chem Phys* **13**:17505–17510 (2011).

142 Luo ZQ, Lim SH, Tian ZQ, Shang JZ, Lai LF, MacDonald B, Fu C, Shen ZX, Yu T and Lin JY, Pyridinic N doped graphene: synthesis, electronic structure, and electrocatalytic property. *J Mater Chem* **21**:8038–8044 (2011).

143 Wang SY, Zhang LP, Xia ZH, Roy A, Chang DW, Baek JB and Dai LM, BCN Graphene as efficient metal-free electrocatalyst for the oxygen reduction reaction. *Angew Chem Int Edn* **51**:4209–4212 (2012).

144 Okamoto Y, First-principles molecular dynamics simulation of O-2 reduction on nitrogen-doped carbon. *Appl Surf Sci* **256**:335–341 (2009).

145 Gong KP, Du F, Xia ZH, Durstock M and Dai LM, Nitrogen-doped carbon nanotube arrays with high electrocatalytic activity for oxygen reduction. *Science* **323**:760–764 (2009).

146 Sun XJ, Zhang YW, Song P, Pan J, Zhuang L, Xu WL and Xing W, Fluorine-doped carbon blacks: highly efficient metal-free electrocatalysts for oxygen reduction reaction. *ACS Catal* **3**:1726–1729 (2013).

147 Yao Z, Nie HG, Yang Z, Zhou XM, Liu Z and Huang SM, Catalyst-free synthesis of iodine-doped graphene via a facile thermal annealing process and its use for electrocatalytic oxygen reduction in an alkaline medium. *Chem Commun* **48**:1027–1029 (2012).

148 Liu ZW, Peng F, Wang HJ, Yu H, Zheng WX and Yang JA, Phosphorus-doped graphite layers with high electrocatalytic activity for the O-2 reduction in an alkaline medium. *Angew Chem Int Ed* **50**:3257–3261 (2011).

149 Yang LJ, Jiang SJ, Zhao Y, Zhu L, Chen S, Wang XZ, Wu Q, Ma J, Ma YW and Hu Z, Boron-doped carbon nanotubes as metal-free electrocatalysts for the oxygen reduction reaction. *Angew Chem Int Ed* **50**:7132–7135 (2011).

150 Yang Z, Yao Z, Li GF, Fang GY, Nie HG, Liu Z, Zhou XM, Chen X and Huang SM, Sulfur-doped graphene as an efficient metal-free cathode catalyst for oxygen reduction. *ACS Nano* **6**:205–211 (2012).
151 Zhang LP and Xia ZH, Mechanisms of oxygen reduction reaction on nitrogen-doped graphene for fuel cells. *J Phys Chem C* **115**:11170–11176 (2011).
152 Kong XK, Chen QW and Sun ZY, Enhanced oxygen reduction reactions in fuel cells on H-decorated and B-substituted graphene. *Chemphyschem* **14**:514–519 (2013).
153 Zheng Y, Jiao Y, Ge L, Jaroniec M and Qiao SZ, Two-step boron and nitrogen doping in graphene for enhanced synergistic catalysis. *Angew Chem Int Ed* **52**:3110–3116 (2013).
154 Choi CH, Park SH and Woo SI, Phosphorus-nitrogen dual doped carbon as an effective catalyst for oxygen reduction reaction in acidic media: effects of the amount of P-doping on the physical and electrochemical properties of carbon. *J Mater Chem* **22**:12107–12115 (2012).
155 Choi CH, Chung MW, Kwon HC, Park SH and Woo SI, B, N- and P, N-doped graphene as highly active catalysts for oxygen reduction reactions in acidic media. *J Mater Chem A* **1**:3694–3699 (2013).
156 Liang J, Jiao Y, Jaroniec M and Qiao SZ, Sulfur and nitrogen dual-doped mesoporous graphene electrocatalyst for oxygen reduction with synergistically enhanced performance. *Angew Chem Int Ed* **51**:11496–11500 (2012).
157 Choi CH, Chung MW, Park SH and Woo SI, Additional doping of phosphorus and/or sulfur into nitrogen-doped carbon for efficient oxygen reduction reaction in acidic media. *Phys Chem Chem Phys* **15**:1802–1805 (2013).
158 Masa J, Zhao AQ, Xia W, Sun ZY, Mei B, Muhler M and Schuhmann W, Trace metal residues promote the activity of supposedly metal-free nitrogen-modified carbon catalysts for the oxygen reduction reaction. *Electrochem Commun* **34**:113–116 (2013).
159 Batchelor-McAuley C, Wildgoose GG, Compton RG, Shao LD and Green MLH, Copper oxide nanoparticle impurities are responsible for the electroanalytical detection of glucose seen using multiwalled carbon nanotubes. *Sensor Actuat B - Chem* **132**:356–360 (2008).
160 Dai X, Wildgoose GG and Compton RG, Apparent 'electrocatalytic' activity of multiwalled carbon nanotubes in the detection of the anaesthetic halothane: occluded copper nanoparticles. *Analyst* **131**:901–906 (2006).
161 Niu W, Li L, Liu X, Wang N, Liu J, Zhou W, Tang Z and Chen S, Mesoporous N-doped carbons prepared with thermally removable nanoparticle templates: an efficient electrocatalyst for oxygen reduction reaction. *J Am Chem Soc* **137**:5555–5562 (2015).
162 Jafri RI, Rajalakshmi N and Ramaprabhu S, Nitrogen doped graphene nanoplatelets as catalyst support for oxygen reduction reaction in proton exchange membrane fuel cell. *J Mater Chem* **20**:7114–7117 (2010).
163 Wang RY, Higgins DC, Hoque MA, Lee D, Hassan F and Chen ZW, Controlled growth of platinum nanowire arrays on sulfur doped graphene as high performance electrocatalyst. *Sci Rep* **3**:2431 (2013).
164 Bai JC, Zhu QQ, Lv ZX, Dong HZ, Yu JH and Dong LF, Nitrogen-doped graphene as catalysts and catalyst supports for oxygen reduction in both acidic and alkaline solutions. *Int J Hydrogen Energy* **38**:1413–1418 (2013).
165 Vinayan BP, Nagar R, Rajalakshmi N and Ramaprabhu S, Novel platinum-cobalt alloy nanoparticles dispersed on nitrogen-doped graphene as a cathode electrocatalyst for PEMFC applications. *Adv Funct Mater* **22**:3519–3526 (2012).
166 Parvez K, Yang SB, Hernandez Y, Winter A, Turchanin A, Feng XL and Mullen K, Nitrogen-doped graphene and its iron-based composite as efficient electrocatalysts for oxygen reduction reaction. *ACS Nano* **6**:9541–9550 (2012).
167 Yu DB, Yao JF, Qiu L, Wu YZ, Li LX, Feng Y, Liu Q, Li D and Wang HT, The synergetic effect of N-doped graphene and silver nanowires for high electrocatalytic performance in the oxygen reduction reaction. *RSC Adv* **3**:11552–11555 (2013).
168 Wang TY, Gao DL, Zhuo JQ, Zhu ZW, Papakonstantinou P, Li Y and Li MX, Size-dependent enhancement of electrocatalytic oxygen-reduction and hydrogen-evolution performance of MoS2 particles. *Chem - Eur J* **19**:11939–11948 (2013).
169 Chatterjee S, Sengupta K, Dey S and Dey A, Ammonium tetrathiomolybdate: a versatile catalyst for hydrogen evolution reaction from water under ambient and hostile conditions. *Inorg Chem* **52**:14168–14177 (2013).
170 Radisavljevic B, Radenovic A, Brivio J, Giacometti V and Kis A, Single-layer MoS2 transistors. *Nat Nanotechnol* **6**:147–150 (2011).
171 Matte HSSR, Gomathi A, Manna AK, Late DJ, Datta R, Pati SK and Rao CNR, MoS2 and WS2 analogues of graphene. *Angew Chem Int Ed* **49**:4059–4062 (2010).
172 Late DJ, Liu B, Matte HSSR, Rao CNR and Dravid VP, Rapid characterization of ultrathin layers of chalcogenides on SiO2/Si substrates. *Adv Funct Mater* **22**:1894–1905 (2012).
173 Castellanos-Gomez A, Barkelid M, Goossens AM, Calado VE, van der Zant HSJ and Steele GA, Laser-thinning of MoS2: on demand generation of a single-layer semiconductor. *Nano Lett* **12**:3187–3192 (2012).
174 Coleman JN, Lotya M, O'Neill A, Bergin SD, King PJ, Khan U, Young K, Gaucher A, De S, Smith RJ, Shvets IV, Arora SK, Stanton G, Kim HY, Lee K, Kim GT, Duesberg GS, Hallam T, Boland JJ, Wang JJ, Donegan JF, Grunlan JC, Moriarty G, Shmeliov A, Nicholls RJ, Perkins JM, Grieveson EM, Theuwissen K, McComb DW, Nellist PD and Nicolosi V, Two-dimensional nanosheets produced by liquid exfoliation of layered materials. *Science* **331**:568–571 (2011).
175 Rao CNR, Maitra U and Waghmare UV, Extraordinary attributes of 2-dimensional MoS2 nanosheets. *Chem Phys Lett* **609**:172–183 (2014).
176 Roxlo CB, Daage M, Leta DP, Liang KS, Rice S, Ruppert AF and Chianelli RR, Catalytic defects at molybdenum-disulfide edge planes. *Solid State Ionics* **22**:97–104 (1986).
177 Kibsgaard J, Chen ZB, Reinecke BN and Jaramillo TF, Engineering the surface structure of MoS2 to preferentially expose active edge sites for electrocatalysis. *Nat Mater* **11**:963–969 (2012).
178 Daage M and Chianelli M, Structure function relation in molybdenum sulfide catalyst the rim edge model. *J Catal* **149**:414–427 (1994).
179 Camachobragado G, Elechiguerra J, Olivas A, Fuentes S, Galvan D and Yacaman M, Structure and catalytic properties of nanostructured molybdenum sulfides. *J Catal* **234**:182–190 (2005).
180 Tauster SJ, Pecoraro TA and Chianelli RR, Structure and properties of molybdenum sulfide - correlation of O-2 chemisorption with hydrodesulfurization activity. *J Catal* **63**:515–519 (1980).
181 Chianelli RR, Ruppert AF, Behal SK, Kear BH, Wold A and Kershaw R, The reactivity of Mos2 single-crystal edge planes. *J Catal* **92**:56–63 (1985).
182 Gao MR, Jiang J and Yu SH, Solution-based synthesis and design of late transition metal chalcogenide materials for oxygen reduction reaction (ORR). *Small* **8**:13–27 (2012).

